JEM Journal of Experimental Medicine

ARTICLE

C-type lectin Mincle mediates cell death–triggered inflammation in acute kidney injury

Miyako Tanaka[1,2*], Marie Saka-Tanaka[1,3*], Kozue Ochi[1,2], Kumiko Fujieda[1,2], Yuki Sugiura[4], Tomofumi Miyamoto[5], Hiro Kohda[1,2], Ayaka Ito[1,2], Taiki Miyazawa[6], Akira Matsumoto[6], Seiichiro Aoe[7], Yoshihiro Miyamoto[8], Naotake Tsuboi[3,9], Shoichi Maruyama[3], Makoto Suematsu[4], Sho Yamasaki[10], Yoshihiro Ogawa[1,11,12,13], and Takayoshi Suganami[1,2]

Accumulating evidence indicates that cell death triggers sterile inflammation and that impaired clearance of dead cells causes nonresolving inflammation; however, the underlying mechanisms are still unclear. Here, we show that macrophage-inducible C-type lectin (Mincle) senses renal tubular cell death to induce sustained inflammation after acute kidney injury in mice. *Mincle*-deficient mice were protected against tissue damage and subsequent atrophy of the kidney after ischemia–reperfusion injury. Using lipophilic extract from the injured kidney, we identified β-glucosylceramide as an endogenous Mincle ligand. Notably, free cholesterol markedly enhanced the agonistic effect of β-glucosylceramide on Mincle. Moreover, β-glucosylceramide and free cholesterol accumulated in dead renal tubules in proximity to Mincle-expressing macrophages, where Mincle was supposed to inhibit clearance of dead cells and increase proinflammatory cytokine production. This study demonstrates that β-glucosylceramide in combination with free cholesterol acts on Mincle as an endogenous ligand to induce cell death–triggered, sustained inflammation after acute kidney injury.

Introduction

Nonresolving sustained inflammation is the common molecular basis underlying a variety of chronic disease conditions, including noninfectious diseases such as atherosclerosis, metabolic syndrome, and cancer (Serhan et al., 2007). As a result of chronic inflammation, the number of parenchymal cells is decreased, homeostatic interactions between parenchymal and stromal cells are altered, and physiological structures in each organ are destroyed, all of which eventually lead to tissue dysfunction. However, it is not fully understood how the inflammatory process persists or the resolution phase is impaired. Several lines of evidence suggest that cell death plays a critical role in sterile inflammation (termed "necroinflammation"; Mulay et al., 2016). For instance, dead or severely damaged cells secrete damage-associated molecular patterns (DAMPs), which activate pattern recognition receptors such as Toll-like receptors to induce inflammatory signaling (Chen and Nuñez, 2010; Miyake, 2007). In addition, clearance of dead cells (efferocytosis) is involved in resolution of inflammation (Kasikara et al., 2018; Nagata and Tanaka, 2017), and impaired efferocytosis exacerbates autoimmune diseases and atherosclerosis (Kojima et al., 2016; Lu and Lemke, 2001). However, how cell death induces sustained inflammation in pathological conditions remains to be fully elucidated.

Acute kidney injury (AKI), a common clinical condition in which kidney function rapidly declines, is associated with high mortality, longer hospital stays, and high medical costs. Kidney function recovers in approximately half of AKI cases, suggesting that the organ has intrinsic repair capacity. In contrast, AKI survivors are at risk of developing chronic kidney disease (CKD), suggesting that tissue damage may accumulate in the kidney. In

[1]Department of Molecular Medicine and Metabolism, Research Institute of Environmental Medicine, Nagoya University, Nagoya, Japan; [2]Department of Immunometabolism, Nagoya University Graduate School of Medicine, Nagoya, Japan; [3]Department of Nephrology, Nagoya University Graduate School of Medicine, Nagoya, Japan; [4]Department of Biochemistry, Keio University School of Medicine, Tokyo, Japan; [5]Department of Natural Products Chemistry, Graduate School of Pharmaceutical Sciences, Kyushu University, Fukuoka, Japan; [6]Institute of Biomaterials and Bioengineering, Tokyo Medical and Dental University, Tokyo, Japan; [7]Department of Home Economics, Otsuma Women's University, Tokyo, Japan; [8]Division of Genomic Diagnosis and Healthcare, National Cerebral and Cardiovascular Center, Suita, Japan; [9]Department of Nephrology, Fujita Health University School of Medicine, Toyoake, Japan; [10]Department of Molecular Immunology, Research Institute for Microbial Diseases, Osaka University, Osaka, Japan; [11]Department of Medicine and Bioregulatory Science, Graduate School of Medical Sciences, Kyushu University, Fukuoka, Japan; [12]Department of Molecular and Cellular Metabolism, Graduate School of Medical and Dental Sciences, Tokyo Medical and Dental University, Tokyo, Japan; [13]Japan Agency for Medical Research and Development, Core Research for Evolutional Science and Technology, Tokyo, Japan.

*M. Tanaka and M. Saka-Tanaka contributed equally to this paper; Correspondence to Takayoshi Suganami: suganami@riem.nagoya-u.ac.jp; Yoshihiro Ogawa: yogawa@intmed3.med.kyushu-u.ac.jp.

AKI, damage to proximal tubules occurs in the corticomedullary junction, followed by intensive infiltration of inflammatory cells such as neutrophils and macrophages, and then surviving proximal tubules massively proliferate to restore renal structure and function (Basile et al., 2012). During this process, various cell types such as proximal tubular cells, inflammatory cells, and fibroblasts interact with each other through secreted factors, including DAMPs. However, it remains unclear how dead tubular cells are recognized by immune cells and involved in the pathogenesis after the initial insult.

Macrophage-inducible C-type lectin (Mincle) is a pattern recognition receptor expressed in innate immune cells such as macrophages and neutrophils (Lee et al., 2012; Matsumoto et al., 1999). Recent studies revealed the role of Mincle in infectious diseases; it recognizes trehalose-6,6′-dimycolate (TDM), a mycobacterial cell wall glycolipid, to induce production of proinflammatory cytokines and chemokines and thus protects against *Mycobacterium tuberculosis* infection (Ishikawa et al., 2009). Mincle also senses cell death, suggesting a role in sterile inflammation (Yamasaki et al., 2008). In this regard, we previously reported that Mincle expression is localized to macrophages surrounding dead or dying adipocytes during the development of obesity, where Mincle accelerates adipocyte death–triggered chronic inflammation in visceral adipose tissue to induce systemic insulin resistance (Tanaka et al., 2014). In the aftermath, evidence has accumulated suggesting the proinflammatory role of Mincle in noninfectious pathology (Greco et al., 2016; Lv et al., 2017; Seifert et al., 2016; Zhou et al., 2016). However, little is known about how Mincle recognizes dead cells under pathological conditions in vivo and how Mincle regulates necroinflammation.

Here, we show that *Mincle* deficiency protects against tissue damage and subsequent atrophy of the kidney after ischemia–reperfusion injury, an experimental model of ischemic AKI. Non-target lipidomics analysis using lipophilic extract from the injured kidney reveals that β-glucosylceramide is an endogenous Mincle ligand in the AKI model. Interestingly, free cholesterol markedly enhances β-glucosylceramide–induced Mincle activation, although free cholesterol per se does not directly act on murine Mincle. Moreover, *Mincle* expression is localized to macrophages in proximity to dead renal tubules, where β-glucosylceramide and free cholesterol accumulate. Thus, Mincle is thought to induce proinflammatory cytokine production and inhibit dead cell clearance, thereby contributing to renal atrophy. This study demonstrates that Mincle recognizes its endogenous ligand derived from dead tubular cells and mediates cell death–triggered, sustained inflammation after AKI.

Results

Mincle-deficient mice are protected against renal injury after ischemia–reperfusion

In this study, we induced ischemia–reperfusion injury of the kidney and collected samples at several time points corresponding to the acute, reparative, and late phases (Fig. 1 A). We first examined the mortality of *Mincle*-deficient (KO) and WT mice for up to 6 d after renal ischemia–reperfusion injury. Although about half of the WT mice died during this period, all KO mice lived (Fig. 1 B). On day 1 (Fig. S1 A), although *Mincle* mRNA expression was markedly increased by AKI, we observed no apparent difference in renal function, tissue damage, neutrophil infiltration, and mRNA expression of proinflammatory cytokines and chemokines between KO and WT mice (Fig. S1, B–E).

We then examined the same parameters on day 3, when the repair process began (Fig. 1, C–F). Serum concentrations of blood urea nitrogen (BUN) were significantly lower in KO mice than in WT mice (Fig. 1 C). In parallel with the acute tubular necrosis (ATN) score (Fig. 1 D), the area immunostained for kidney injury molecule 1 (KIM-1), a damaged tubular marker, was significantly low in KO mice compared with WT mice (Fig. 1 E). Up-regulation of *Mincle* mRNA levels persisted in the kidney at this time point (Fig. 1 F). Moreover, mRNA up-regulation of macrophage marker *Emr1* (F4/80); tubular damage marker *Havcr1* (KIM-1); proinflammatory cytokines such as *Il6* and *Tnfa* (tumor necrosis factor–α); and chemokine *Ccl2* (monocyte chemoattractant protein 1; MCP-1) was markedly suppressed in KO mice (Fig. 1 F). By measuring mRNA levels in each sorted cell type from the kidney, we confirmed the cellular source of each mRNA; *Mincle*, *Ccl2*, and *Tnfa* were predominantly expressed in macrophages, and *Havcr1* and *Il6* were mainly from nonimmune cells (data not shown). Consistent with mRNA expression, the number of infiltrating F4/80^{lo} macrophages tended to be low in KO mice relative to WT mice on day 3, whereas there was no appreciable difference in F4/80^{hi} macrophages between the genotypes (Fig. 1 G).

Microarray analysis revealed that the overlap between the genes up-regulated in injured kidney versus sham kidney in WT mice and the genes down-regulated in injured kidney in KO mice versus WT mice included inflammation-related pathways on day 3 (Fig. S2), although this overlap was quite small on day 1. Collectively, these results demonstrate that *Mincle* deficiency protects against renal injury, particularly in the reparative phase, after ischemia–reperfusion injury.

Mincle in bone marrow cells contributes to renal injury after ischemia–reperfusion

We next performed bone marrow transplantation experiments to confirm the role of Mincle in immune cells. After 4 wk of recovery, four groups of bone marrow–chimeric mice were subjected to renal ischemia–reperfusion injury and analyzed 3 d later (Fig. 2 A). In the mice harboring WT bone marrow cells, *Mincle* mRNA expression was markedly increased in the injured kidney compared with the sham-operated kidney (Fig. 2 B). On the other hand, in mice harboring KO bone marrow cells, *Mincle* mRNA expression was negligible (Fig. 2 B), suggesting that *Mincle* was expressed exclusively in bone marrow–derived immune cells in the injured kidney. As expected, bone marrow–chimeric KO mice were protected against renal injury after ischemia–reperfusion (Fig. 2, C and D). In contrast, *Mincle* overexpression in bone marrow cells exacerbated renal injury (Fig. 2, C and E). These results confirm that Mincle in bone marrow–derived immune cells play a critical role in renal ischemia–reperfusion injury.

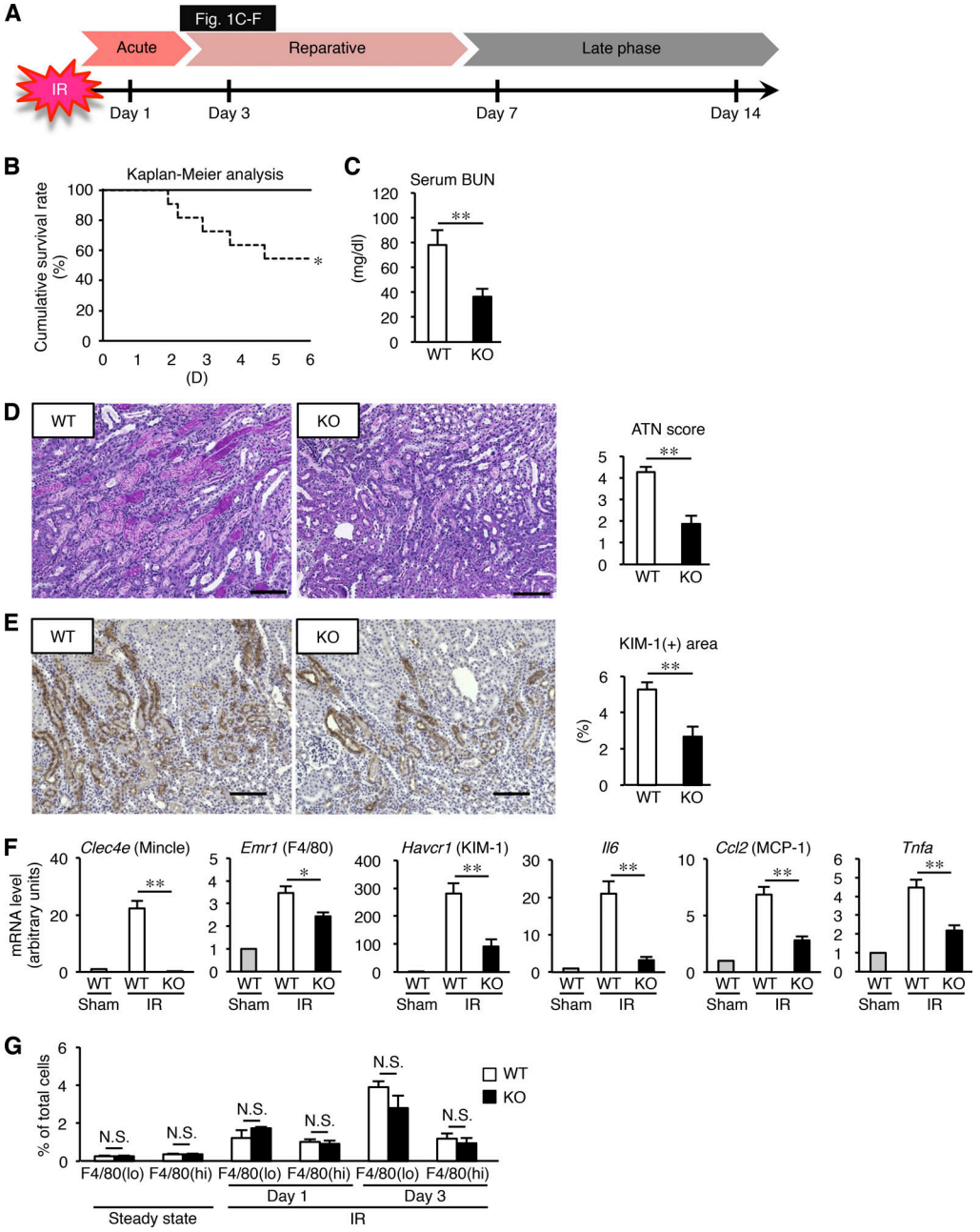

Figure 1. **Amelioration of inflammation and injury after renal ischemia–reperfusion in *Mincle*-deficient mice. (A)** Experimental time course of this study. *Mincle*-deficient (KO) and WT mice were subjected to renal ischemia–reperfusion injury (ischemia for 30 min) after resection of the right kidney and were analyzed at the indicated time points. $n = 6$; unpaired t test. **(B)** Cumulative survival rate of KO and WT mice after renal ischemia–reperfusion. D, days after renal ischemia–reperfusion injury. $n = 11$. *, $P < 0.05$. **(C–E)** Evaluation of renal inflammation and injury on day 3 after renal ischemia–reperfusion. $n = 7–9$. **(C)** Serum BUN concentrations. Values are mean ± SEM. **, $P < 0.01$; unpaired t test. **(D)** Representative images of periodic acid–Schiff staining of the kidney outer medulla, along with ATN scores. Scale bars, 100 µm. Values are mean ± SEM. **, $P < 0.01$; unpaired t test. **(E)** Representative images of KIM-1 immunostaining of the kidney outer medulla and the KIM-1–positive area. Scale bars, 100 µm. Values are mean ± SEM. **, $P < 0.01$; unpaired t test. **(F)** mRNA expression of genes related to macrophages, inflammation, and tubular injury. Values are mean ± SEM. *, $P < 0.05$; **, $P < 0.01$; ANOVA. IR, ischemia–reperfusion injured kidney; Sham, sham-operated kidney. **(G)** Percentage of F4/80^{lo} and F4/80^{hi} macrophages (CD45$^+$ CD11b$^+$ F4/80^{lo} and CD45$^+$ CD11b$^+$ F4/80^{hi}, respectively) in total renal cells at steady state and on indicated days after renal ischemia–reperfusion injury. Values are mean ± SEM. $n = 3–4$. N.S., not significant; ANOVA. Data shown are representative of at least three independent experiments.

Characterization of Mincle-expressing cells infiltrating the injured kidney

Since macrophages and neutrophils are supposed to express Mincle in the injured kidney, we examined mRNA expression of *Cxcr2* (a marker for neutrophils) and *Emr1* and found that macrophages were responsible for *Mincle* expression on day 3 (Fig. S1 F). Next, we employed *Cx3cr1*$^{CreERT2/+}$:*Rosa26*$^{tdTomato/tdTomato}$ mice (Reed-Geaghan et al., 2020), in which tissue resident macrophages in the kidney were labeled with tdTomato after tamoxifen injection while circulating monocytes were not.

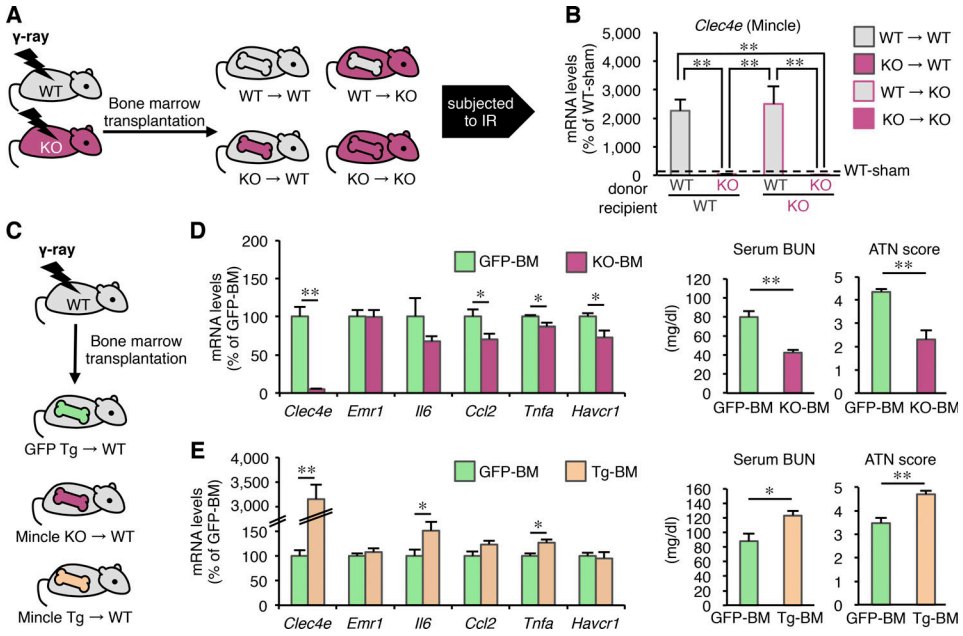

Figure 2. **Role of Mincle in bone marrow–derived cells in inflammation and injury after renal ischemia–reperfusion. (A)** Experimental protocol of bone marrow transplantation experiments. Bone marrow cells from KO and WT mice were transplanted to lethally irradiated KO and WT mice. After a 4-wk recovery period, mice were subjected to renal ischemia–reperfusion injury and analyzed on day 3. **(B)** Expression levels of *Mincle* mRNA in kidneys from each group. Values are mean ± SEM. n = 4–6. **, P < 0.01; ANOVA. **(C)** Experimental protocol to elucidate the role of Mincle in bone marrow–derived cells after renal ischemia–reperfusion injury. Bone marrow cells from KO, Mincle Tg, and GFP Tg mice were transplanted into lethally irradiated WT mice. **(D and E)** Effect of *Mincle* deficiency (D) and overexpression (E) in bone marrow–derived cells on mRNA expression of the genes related to macrophages, inflammation, and tubular injury, along with serum BUN concentrations and ATN scores. BM, bone marrow. Values are mean ± SEM. n = 6. *, P < 0.05; **, P < 0.01; unpaired t test. Data shown are representative of at least two independent experiments.

Using these mice, we confirmed that circulating monocytes contributed to F4/80^{lo} macrophages in the injured kidney on day 3 (Fig. 3 A). Then, we sorted CD45$^+$ CD11b$^+$ F4/80^{lo} and CD45$^+$ CD11b$^+$ F4/80^{hi} cells to examine which macrophage subtype expresses Mincle (Fig. 3 B). As a result, *Mincle* was predominantly expressed in F4/80^{lo} macrophages, which exhibited mixed phenotypes with high expression of proinflammatory (*Il6*, *Cxcl2*, and nitric oxide synthase 2 [*Nos2*; inducible nitric oxide synthase or iNOS]) and anti-inflammatory (arginase 1 [*Arg-1*], interferon regulatory factor 4 [*Irf4*], and macrophage galactose-type lectin 1 [*Mgl1*]) markers (Fig. 3 C), suggesting a phenotypic change from proinflammatory to anti-inflammatory properties in the reparative phase in an AKI model as reported (Lee et al., 2011). Moreover, in situ hybridization analysis revealed that *Mincle*-expressing cells surrounded the severely damaged tubules with intraluminal debris and *Mincle* mRNA was positive in only a subset of macrophages infiltrating the injured kidney (Fig. 3 D). Flow cytometry detected a small cluster of Mincle-positive cells, comprising F4/80^{lo} macrophages mildly expressing Ly6C (Fig. 3 E). These cells showed a unique phenotype, with high expression of *Il6*, *Arg-1*, and *Mcr1*. Collectively, our data indicate that Mincle is selectively expressed in a small subset of F4/80^{lo} macrophages with a unique phenotype, which are localized surrounding the damaged tubules.

Mincle is involved in AKI-to-CKD transition

Because *Mincle* expression persisted in the late phase (on day 7 after ischemia–reperfusion injury; Fig. 1 A and Fig. 4, A and B), we next sought to determine whether Mincle is involved in the AKI-to-CKD transition. We focused on cell death, since various types of cell death such as apoptosis and regulated necrosis are involved in the pathogenesis of AKI (Linkermann et al., 2014; Wei et al., 2013). Immunofluorescence analysis revealed that F4/80-positive macrophages surrounded TdT-mediated dUTP nick-end labeling (TUNEL)– or cleaved caspase-3–positive dead tubules in the corticomedullary junction area, whereas only a few macrophages were located in proximity to mature proximal tubules that immunostained for lotus tetragonolobus lectin (LTL; Fig. 4 C). In this setting, mRNA expression and immunostaining of KIM-1 was markedly suppressed in KO mice relative to WT mice (Fig. 4, B and D). The number of TUNEL-positive cells was also reduced in KO mice (Fig. 4 E). On the other hand, up-regulation of mRNA levels of regeneration-related genes (*Sox9*, *Wnt7b*, and *Pax8*) was rather lower in KO mice than in WT mice (Fig. 4 B), suggesting that regeneration may not contribute to prevention of sustained inflammation and tubular damage in the late phase in KO mice. Moreover, the ratio of injured to contralateral kidney weight was significantly higher in KO mice on day 14 (Fig. 5, A and B), suggesting prevention of renal atrophy in the late phase. Consistent with this, the area positive for LTL in the injured kidney was well preserved, and the number of TUNEL-positive cells was low in KO mice at this time point (Fig. 5, C and D). These findings suggest that Mincle contributes to sustained tubular cell death and subsequent renal atrophy in the late phase after renal ischemia–reperfusion injury.

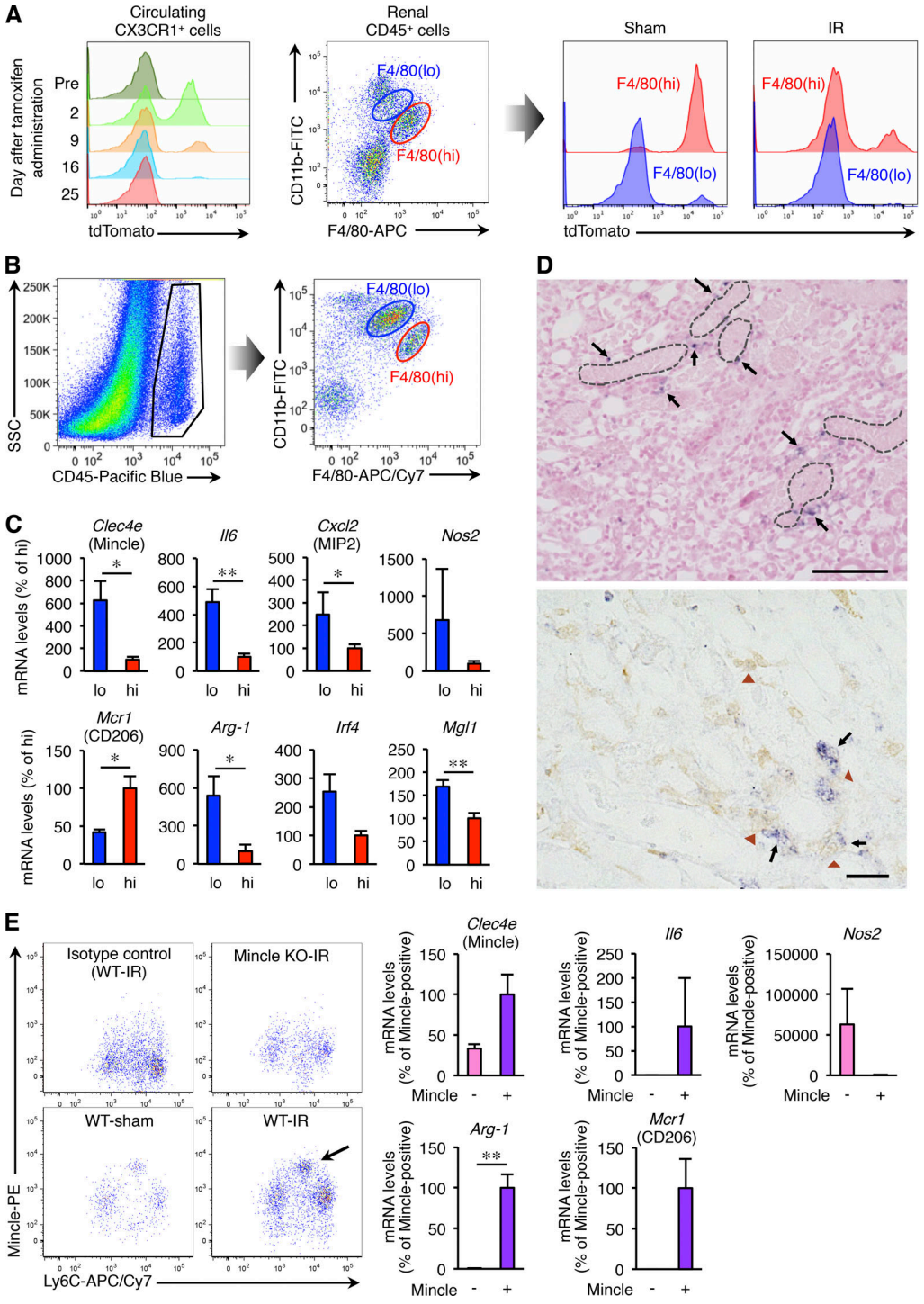

Figure 3. **Characterization of Mincle-expressing macrophages infiltrating the injured kidney. (A)** Lineage tracing of circulating monocytes and resident macrophages of the kidney. *Cx3cr1*$^{CreERT2/+}$: *Rosa26*$^{tdTomato/tdTomato}$ mice were orally administered 100 mg/kg of tamoxifen for 5 consecutive days. Before and after administration, expression of tdTomato on circulating CX3CR1-expressing cells was determined. After 4 wk, these mice were subjected to renal ischemia–reperfusion injury and evaluated using flow cytometry tdTomato expression of F4/80^{lo} and F4/80^{hi} macrophages on day 3. **(B)** FACS analysis of renal macrophages in the injured kidney on day 3 after ischemia–reperfusion injury. CD45-positive cells were divided into the F4/80^{lo} and F4/80^{hi} groups. SSC, side scatter. **(C)** mRNA expression of *Mincle*, *Il6*, *Cxcl2*, *Nos2*, *Mrc1*, *Arg-1*, *Irf4*, and *Mgl1* in sorted F4/80^{lo} and F4/80^{hi} macrophages. Values are mean ± SEM. n = 5. *, P < 0.05; **, P < 0.01; unpaired t test. **(D)** Representative images of in situ hybridization of *Mincle* in the injured kidney on day 3 after ischemia–reperfusion injury. Black arrows, *Mincle*-expressing cells; dotted lines, intraluminal debris; brown arrowheads, macrophages (Iba1-positive cells). Scale bars, 50 µm. **(E)** FACS analysis of Mincle-expressing cells in the injured kidney. F4/80^{lo} macrophages were analyzed using antibodies for Mincle and Ly6C. Mincle-positive and -negative cells in F4/80^{lo} macrophages were sorted and subjected to real-time PCR analysis. Arrow indicates Mincle-positive macrophages. Values are mean ± SEM. n = 3. **, P < 0.01; unpaired t test. Data shown are representative of at least two independent experiments.

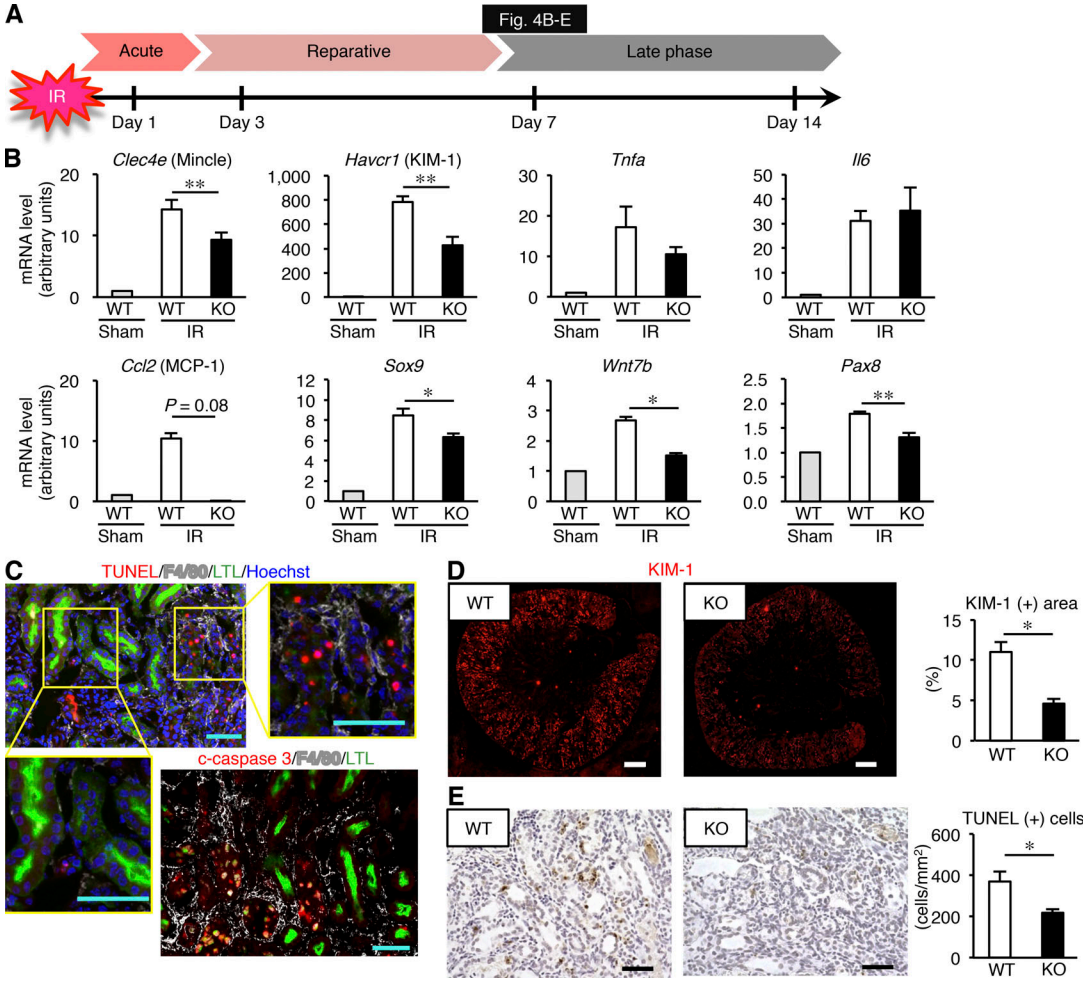

Figure 4. **Amelioration of sustained inflammation and tubular damage after renal ischemia–reperfusion in *Mincle*-deficient mice. (A)** Experimental time course of this study. KO and WT mice were subjected to renal ischemia–reperfusion injury (ischemia for 35 min) without resecting the right kidney and were analyzed on day 7. **(B)** mRNA expression of genes related to tubular injury, inflammation, and regeneration in the injured kidney. **(C)** Representative images of immunofluorescence staining of the injured kidney. Red, white, green, and blue indicate TUNEL or cleaved caspase-3, F4/80, LTL (a marker for mature proximal tubules), and nuclear DNA, respectively. Insets: High-magnification images of injured proximal tubules (left) and dead tubules (right). Scale bars, 50 µm. **(D)** Representative images of KIM-1 immunofluorescence staining and the KIM-1–positive area in the injured kidney. Scale bars, 500 µm. **(E)** Representative images of TUNEL staining and the number of TUNEL-positive cells in the injured kidney. Scale bars, 50 µm. Data shown are representative of at least three independent experiments. Values are mean ± SEM. $n = 5$. *, $P < 0.05$; **, $P < 0.01$; ANOVA.

Mincle regulates clearance of dead cells

Since several lines of evidence point to the role of Mincle in the phagocytosis of pathogens (Haider et al., 2019; Patin et al., 2017a), we next sought to elucidate how Mincle is involved in the clearance of dead cells. Mincle stimulation in cultured macrophages using TDM, an exogenous Mincle ligand derived from *M. tuberculosis* (Ishikawa et al., 2009), was previously shown to increase mRNA levels of inflammation-related genes such as *Il6* (Fig. 6 A). In addition, we found that mRNA expression of the genes related to phagocytosis (MER proto-oncogene, tyrosine kinase [*Mertk*], *Gas6*, *Mfge8*, and *Intgb5*) was markedly suppressed by treatment with TDM in WT macrophages, whereas these effects were abolished in KO macrophages (Fig. 6 A). Phagocytosis assay using necrotic cell debris and apoptotic cells revealed that Mincle stimulation effectively suppressed phagocytotic activity (engulfment and binding of dead cells; Fig. 6, B and C). Contrary to our expectation, these effects were only partly suppressed in KO macrophages (Fig. 6, B and C), suggesting the possible involvement of a Mincle-independent pathway.

To determine a molecular mechanism, we focused on liver X receptors (LXRs), which induce phagocytosis-related genes such as *Mertk* while repressing proinflammatory cytokines such as *Tnfa* (Ito et al., 2015). We examined the signaling crosstalk of Mincle and LXR and found that Mincle stimulation counteracted LXR signaling with regard to mRNA expression of *Mertk* and *Tnfa* (Fig. 6 D), phagocytosis of cell debris (Fig. 6 E), and cell surface expression of MerTK (Fig. 6 F). These findings suggest that Mincle signaling in macrophages impairs clearance of dead cells, potently contributing to sustained inflammation after renal ischemia–reperfusion injury.

Identification of endogenous Mincle ligands in the injured kidney

We next screened for endogenous Mincle ligands released from dead or dying tubular epithelial cells in the injured kidney after

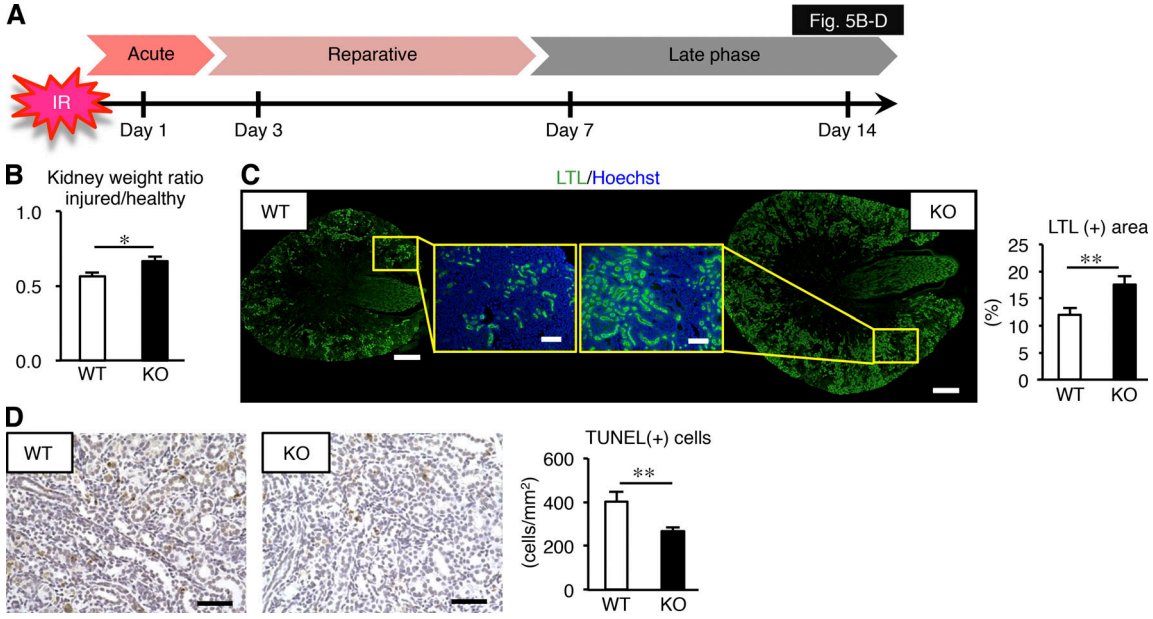

Figure 5. **Prevention of renal atrophy after ischemia–reperfusion injury in *Mincle*-deficient mice. (A)** Experimental time course of this study. KO and WT mice were subjected to renal ischemia–reperfusion injury (ischemia for 35 min) without resecting the right kidney and were analyzed on day 14. **(B)** Ratio of injured kidney weight to healthy (sham-operated) kidney weight. Values are mean ± SEM. **(C)** Representative images of LTL staining of and the LTL-positive area in the injured kidney. Insets: High-magnification images of the corticomedullary junction area of KO (right) and WT (left) mice. Scale bars, 500 µm and 100 µm in low- and high-power fields, respectively. Values are mean ± SEM. **(D)** Representative images of TUNEL staining and the number of TUNEL-positive cells in the injured kidney. Scale bars, 50 µm. Data shown are representative of at least three independent experiments. Values are mean ± SEM. *n* = 5. *, P < 0.05; **, P < 0.01; ANOVA.

ischemia–reperfusion. Because the Mincle ligands identified to date are lipids or glycolipids (Behler-Janbeck et al., 2016; Ishikawa et al., 2009; Nagata et al., 2017), we extracted total lipids from the kidney, fractionated them isocratically using different ratios of chloroform and methanol, and subjected them to an NFAT-GFP reporter assay as described (Fig. 7 A; Kiyotake et al., 2015; Nagata et al., 2017; Yamasaki et al., 2008). Fraction 9:1 (eluted by 9:1 chloroform:methanol [vol/vol]) from the injured kidney (ischemia–reperfusion [IR]–9:1) exhibited a remarkable reporter activity relative to fraction 9:1 from sham-operated kidney (sham–9:1; Fig. 7 A). Liquid chromatography–mass spectrometry (LC-MS)–based lipidomics analysis identified several candidate lipid metabolites, including hexosylceramides (β-glucosylceramide and β-galactosylceramide), levels of which were higher in IR–9:1 than in sham–9:1 (Fig. S3 A). Among them, only β-glucosylceramide was capable of increasing reporter cell activity (data not shown). Although β-glucosylceramide has been reported as an endogenous Mincle ligand from cultured dying cells (Nagata et al., 2017), the effect of β-glucosylceramide per se was relatively weak compared with that of IR–9:1 (Fig. 7, A and B).

These findings led us to speculate that some other molecules included in IR–9:1 may enhance the effect of β-glucosylceramide. Considering the high content of free cholesterol in IR–9:1, we found that free cholesterol markedly increased the reporter cell activity induced by β-glucosylceramide (Fig. 7 B). We confirmed these observations using various β-glucosylceramides harboring distinct fatty acid chains and β-galactosylceramide (Fig. 7 C). Of note, free cholesterol was reported to be an endogenous ligand for human Mincle, not for murine Mincle (Kiyotake et al., 2015).

We further investigated whether coexistence of β-glucosylceramide and free cholesterol is required for Mincle activation. In this experiment, NFAT-GFP reporter cells were pretreated with free cholesterol, transferred to different dishes, and then treated with β-glucosylceramide. Such sequential treatment did not show the synergistic effect (Fig. S3 B). In addition to the reporter cell activity, β-glucosylceramide in combination with free cholesterol effectively increased *Il6* mRNA expression in cultured macrophages through Mincle (Fig. 7, D and E). Moreover, Western blot analysis revealed that β-glucosylceramide induced phosphorylation of spleen tyrosine kinase (Syk) through Mincle (Fig. 7 F), similar to the previous report showing the role of the TDM–Mincle–Syk pathway in induction of proinflammatory cytokine expression (Yamasaki et al., 2008). Intracellular staining of phosphorylated Syk using flow cytometry confirmed these results (Fig. 7 G).

Accumulation of β-glucosylceramide and free cholesterol in the injured kidney

Finally, we sought to detect β-glucosylceramide and free cholesterol in the injured kidney after ischemia–reperfusion. LC-MS analysis revealed that the content of hexosylceramides harboring certain types of fatty acids (18:0 and 24:1) was significantly increased in the injured kidney compared with the sham-operated kidney (Fig. 7 H). Given that β-glucosylceramide is an abundant hexosylceramide in various tissues (Nagata et al., 2017), we speculated that β-glucosylceramide, rather than β-galactosylceramide, accumulated as an endogenous Mincle ligand in the injured kidney after ischemia–reperfusion injury.

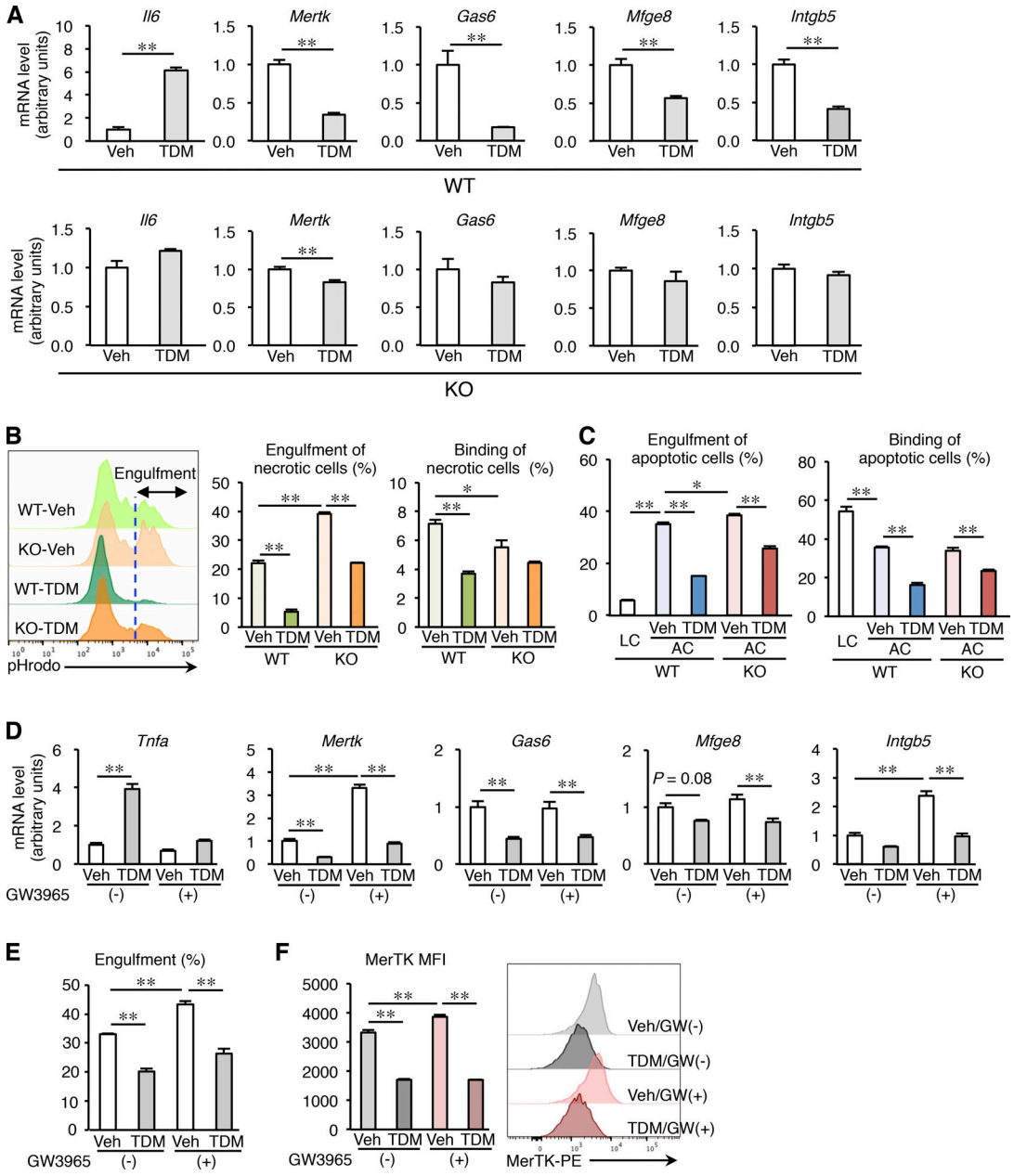

Figure 6. **Mincle-mediated inhibition of macrophage phagocytotic activity in vitro.** Peritoneal macrophages from KO and WT mice were treated with vehicle (Veh, isopropanol) or 2.5 µg/well (24-well plate) of TDM for 24 h. **(A)** mRNA expression of genes related to macrophage phagocytotic activity. Values are mean ± SEM. $n = 4$. **, $P < 0.01$; unpaired t test. **(B)** Effect of TDM on engulfment and binding of necrotic cells by peritoneal macrophages from KO and WT mice. Left: Representative pHrodo staining profile. The blue dashed line indicates the threshold for evaluating engulfment. Middle: Engulfment of necrotic cells. Right: Binding of necrotic cells. Values are mean ± SEM. $n = 3$. *, $P < 0.05$; **, $P < 0.01$; ANOVA. **(C)** Effect of TDM on engulfment and binding of apoptotic cells (ACs) by peritoneal macrophages from KO and WT mice. Living cells (LCs) were used as control. Engulfment (left) and binding (right) of apoptotic cells. Values are mean ± SEM. $n = 3$. *, $P < 0.05$; **, $P < 0.01$; ANOVA. **(D)** Effect of Mincle stimulation on LXR–mediated mRNA expression of genes regulating macrophage phagocytotic activity. Peritoneal macrophages were treated with TDM, GW3965 (an LXR agonist), or both compounds for 24 h. Values are mean ± SEM. $n = 4$. **, $P < 0.01$; ANOVA. **(E)** Phagocytosis assay using cell debris. After treatment with TDM, GW3965, or both compounds, WT peritoneal macrophages were incubated with cell debris for 30 min. Values are mean ± SEM. $n = 4$. **, $P < 0.01$; ANOVA. **(F)** Cell surface expression of MerTK. After treatment with TDM, GW3965, or both compounds, WT peritoneal macrophages were analyzed by flow cytometry. MFI (mean fluorescence intensity) of MerTK and representative histograms for MerTK expression are shown. $n = 4$. **, $P < 0.01$; ANOVA. Data shown are representative of at least three independent experiments.

Imaging MS detected accumulation of hexosylceramides mainly in the corticomedullary junction area (Fig. 7 I). Filipin staining revealed that intratubular aggregation of free cholesterol was scattered in the injured area and surrounded by macrophages (Fig. 7 J) and did not colocalize with damaged tubules positive for KIM-1 staining. Because laminin staining disappeared in the macrophage-infiltrated tubules containing accumulated cholesterol, it is conceivable that these tubules were severely damaged or dead (Fig. 7 K). Taken together with our in vitro data that β-glucosylceramide, not β-galactosylceramide, was capable of

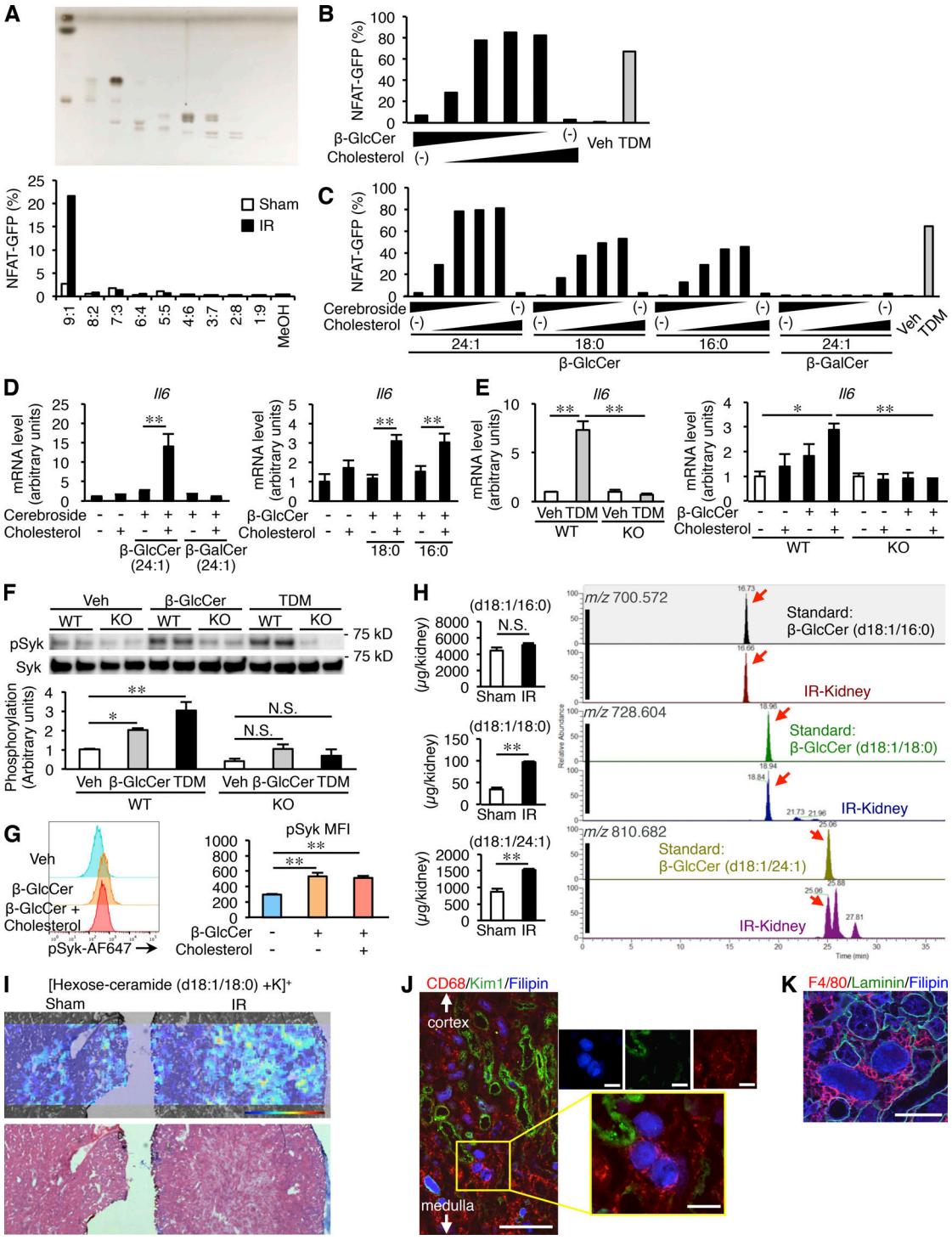

Figure 7. **Identification of endogenous Mincle ligands in the injured kidney. (A)** Screening for endogenous Mincle ligands in an NFAT-GFP reporter assay. Kidney lipid extracts were eluted isocratically with chloroform and methanol by silica gel column chromatography. Each fraction was analyzed by high-perfomance thin-layer chromatography (HPTLC) developed with chloroform-methanol-water (65:25:4, vol/vol/vol). The HPTLC plate was stained by copper acetate–phosphoric acid (upper). Each fraction was coated onto a plate to stimulate NFAT-GFP reporter cells stably expressing Mincle and Fc receptor (FcRγ). The NFAT-GFP induction was assessed by flow cytometry (lower). **(B)** Reporter cell activity of β-glucosylceramide (β-GlcCer; d18:1/24:1; 0–6.7 μg/well, 96-well plate) in combination with free cholesterol (0–6.7 μg/well, 96-well plate). Vehicle (Veh, isopropanol). **(C)** Effects of β-GlcCer with distinct fatty acid chain on reporter cell activity. β-GlcCer (d18:1/24:1), β-GlcCer (d18:1/18:0), β-GlcCer (d18:1/16:0), and β-galactosylceramide (β-GalCer; d18:1/24:1) were evaluated. **(D)** Induction of *Il6* mRNA expression in RAW264 cells stimulated with various types of cerebrosides (0–26.7 μg/well, 24-well plate) for 24 h. Values are mean ± SEM. n = 3–4. **, P < 0.01; ANOVA. **(E)** Induction of *Il6* mRNA expression in KO and WT peritoneal macrophages stimulated with TDM (2.5 μg/well, 24-well plate) or β-GlcCer (d18:1/24:1; 0–26.7 μg/well, 24-well plate) with or without free cholesterol (0–26.7 μg/well) for 24 h. Values are mean ± SEM. n = 4; *, P < 0.05; **, P < 0.01; ANOVA. **(F)** Western blotting analysis of phosphorylation of Syk (pSyk; Tyr525/526) in KO and WT peritoneal macrophages stimulated with TDM (5 μg/well, 12-well plate) or β-GlcCer (d18:1/24:1; 53.3 μg/well, 12-well plate). Values are mean ± SEM. n = 4; *, P < 0.05; **, P < 0.01, N.S., not significant;

ANOVA. **(G)** FACS analysis of phosphorylated Syk (Tyr525/526) in WT peritoneal macrophages stimulated with β-GlcCer (d18:1/24:1) with or without free cholesterol (53.3 µg/well, 12-well plate). *n* = 3; **, P < 0.01, N.S., not significant; ANOVA. **(H)** Measurement of hexosylceramide levels in the kidney on day 3 after renal ischemia–reperfusion using LC-MS/MS. Arrows indicate the respective hexosylceramide species. *n* = 3; **, P < 0.01, N.S., not significant; unpaired *t* test. **(I)** Imaging MS analysis of hexosylceramide (d18:1/18:0) in the kidney on day 3. **(J and K)** Filipin staining of the injured kidney on day 3. Triple staining of the corticomedullary junction area. **(J)** CD68, KIM-1, and Filipin. Insets: High-magnification images of cholesterol aggregation surrounded by macrophages. Scale bars, 200 µm and 50 µm in low- and high-power fields, respectively. **(K)** F4/80, laminin, and Filipin. Scale bar, 50 µm. The image was captured by confocal microscopy. Data shown are representative of at least three independent experiments.

activating Mincle, these findings indicate that β-glucosylceramide in combination with free cholesterol acts on Mincle in the injured kidney following ischemia–reperfusion.

Discussion

Nonresolving inflammation is a critical determinant factor in the progression from AKI to CKD (Ferenbach and Bonventre, 2015; Sato and Yanagita, 2018). Following initial insults, inflammatory responses induced by tubular injury provoke maladaptive tissue repair and additional tubular damage (Mulay et al., 2016). However, the precise mechanism underlying cell death–triggered sustained inflammation remains to be elucidated. Here, we provide evidence that Mincle, a novel sensor of cell death, is involved in this process. In particular, Mincle senses dead tubules to increase proinflammatory cytokine production and decrease dead cell clearance, thereby aggravating a vicious cycle of necroinflammation (Fig. S4). Consistent with this, Mincle deficiency markedly preserved healthy mature proximal tubules in the late phase after renal ischemia–reperfusion injury. In other words, the risk of AKI-to-CKD transition was effectively reduced in *Mincle* KO mice. Although AKI results from various etiologies, including ischemic and toxic insults, the close interaction between severely damaged or dead tubules and immune cells is a common pathogenesis in the reparative phase after an acute destructive event (Huen and Cantley, 2015). Because it is clinically difficult to intervene in the acute phase of AKI (or initial tubular damage), Mincle is a rational therapeutic target for ameliorating the subsequent progression from AKI to CKD.

In this study, we identified an endogenous ligand of Mincle for the first time using in vivo pathological tissue samples. Previously, several glycolipids from *M. tuberculosis* and *Streptococcus pneumoniae* were reported as exogenous Mincle ligands (Behler-Janbeck et al., 2016; Ishikawa et al., 2009). In terms of endogenous Mincle ligands, cholesterol crystals and cholesterol sulfate were identified using healthy liver and skin, respectively (Kiyotake et al., 2015; Kostarnoy et al., 2017). β-glucosylceramide released from dying cultured cells is also an endogenous Mincle ligand (Nagata et al., 2017). In this study, we found that β-glucosylceramide accumulated in the injured kidney is an endogenous ligand for Mincle in the AKI model. Interestingly, a comparison of the effects of β-glucosylceramide on its own and the injured kidney–derived fractionated sample on reporter cell activity led us to find that free cholesterol markedly enhances the effect of β-glucosylceramide on Mincle. Consistent with this, β-glucosylceramide, as well as free cholesterol, accumulates in the severely damaged area of the corticomedullary junction in vivo. To the best of our knowledge, this is the first report to prove that the effect of DAMPs is remarkably increased in the presence of a certain metabolite. Intriguingly, free cholesterol per se does not directly act on murine Mincle (Kiyotake et al., 2015; Kostarnoy et al., 2017). Although it is still unclear how the combination of β-glucosylceramide and free cholesterol showed a drastic effect on Mincle activity, it would be interesting to investigate the spatio-temporal localization of these metabolites after renal ischemia–reperfusion injury.

It is important to determine how Mincle regulates macrophage functions in the pathogenesis of AKI. Yamasaki et al. (2008) previously reported that TDM, a glycolipid in the mycobacterial cell wall, acts on Mincle to activate Syk through association with the Fc receptor, FcRγ, thereby inducing proinflammatory cytokine production. We and others also showed the proinflammatory role of Mincle in noninfectious diseases (Greco et al., 2016; Lv et al., 2017; Seifert et al., 2016; Tanaka et al., 2014; Zhou et al., 2016). This study revealed that Mincle-mediated phagocytosis of dead cells (binding and engulfment) may be involved in sustained inflammation. In this regard, this study provided evidence on the novel role of Mincle in sterile inflammation. Therefore, it is conceivable that Mincle causes sustained inflammation after renal ischemia–reperfusion injury through at least two different mechanisms: induction of tubular cell death and impairment of dead cell clearance. On the flip side, recent studies have pointed to the controversial role of Mincle in pathogen uptake (Patin et al., 2017b; Wells et al., 2008), suggesting ligand or context dependence. Since several lines of evidence indicate the role of Mincle in autophagy during bacterial infection (Pahari et al., 2020; Sharma et al., 2017), it is interesting to examine the molecular mechanism underlying Mincle-mediated regulation of dead cell clearance for future directions. Thus, our data link the previously known pathogenic role of various types of cell death in AKI (Linkermann et al., 2014; Wei et al., 2013) and the role of Mincle in cell death–induced sterile inflammation (Greco et al., 2016; Lv et al., 2017; Seifert et al., 2016; Tanaka et al., 2014; Zhou et al., 2016).

Increasing attention has been paid to the role of macrophage subsets in the progression from acute to chronic inflammation. For instance, a phenotypic switch between M1 and M2 macrophages is observed during the course of renal injury in several experimental models (Meng et al., 2015), whereas it is becoming a consensus that canonical M1 versus M2 macrophages cannot be applicable to pathological conditions in vivo (Baek, 2019). In this study, we found that Mincle is a specific marker for Ly6C^{int} macrophages, a small cluster (~10%) in F4/80^{lo} macrophages in the injured kidney. In this regard, Clements et al. (2016) previously described these Ly6C^{int} macrophages in the reparative phase following infiltration of Ly6C^{hi} proinflammatory macrophages after renal ischemia–reperfusion, whereas their pathophysiologic

role remains to be elucidated. Although macrophage polarization is conceptual, a myriad of surface markers have been reported for each etiology and organ. Indeed, Mincle-expressing macrophages showed a unique phenotype with high expression of classical M1 and M2 markers, which may reflect their complex nature. Namely, it is conceivable that Mincle-expressing macrophages surrounding dead cells regulate classical M1 (production of proinflammatory cytokines) and M2 (clearance of dead cells) functions in the reparative phase after renal ischemia–reperfusion injury. Thus, Mincle-expressing Ly6C^{int} macrophages would be a novel subset that gives rise to cell death–triggered, sustained inflammation in this mouse model of AKI. In addition, an increased number of infiltrating macrophages is supposed to be a major cause of *Mincle* up-regulation in the injured kidney, whereas the inflammatory microenvironment may induce *Mincle* expression through certain intracellular signaling pathways after infiltration of the injured kidney, as its name (macrophage-inducible C-type lectin) implies. Further studies are needed to determine whether Mincle-expressing macrophages originate from a progenitor distinct from other macrophage populations or instead only transiently induce Mincle expression. Nevertheless, this study clearly demonstrates the role of a small number of Mincle-expressing macrophages in the AKI-to-CKD transition.

The microenvironment in which Mincle-expressing macrophages aggregate around dead tubules in the injured kidney is reminiscent of previously known "crown-like structures" in adipose tissue and liver (Itoh et al., 2013; Murano et al., 2008). Such crown-like structures were originally observed in adipose tissue during the development of obesity, in which CD11c-positive macrophages surround dead or dying adipocytes (Lumeng et al., 2008). We previously demonstrated that this structure is a source of proinflammatory and profibrotic factors and thus drives tissue remodeling (Tanaka et al., 2014). We also identified a similar structure in the liver that promotes the progression from simple hepatic steatosis to nonalcoholic steatohepatitis (Itoh et al., 2013; Itoh et al., 2017). Interestingly, macrophages in crown-like structures are positive for Mincle in the injured kidney after ischemia–reperfusion as well as in obese adipose tissue (Tanaka et al., 2014). Accordingly, it is likely that activation of Mincle is a common molecular basis underlying cell death–triggered chronic inflammation. For future directions, it is important to clarify which types of cell death play a critical role in the pathogenesis of each disease condition, including AKI-to-CKD transition.

In summary, we demonstrated that Mincle-expressing macrophages aggregate around dead tubules in the corticomedullary junction area after renal ischemia–reperfusion, where Mincle induces proinflammatory cytokine production and inhibits dead cell clearance, thereby aggravating a vicious cycle of chronic inflammation (Fig. S4). Our data also indicate that β-glucosylceramide derived from dead tubules in combination with free cholesterol is an endogenous ligand for Mincle. Because limited information is available regarding the in situ localization of specific macrophage subsets in inflamed tissues, this study provides evidence that a small subset of macrophages expressing Mincle is localized in proximity to dead tubules and drives cell death–triggered inflammation, thereby promoting the AKI-to-CKD transition.

Materials and methods

Reagents

All reagents were purchased from Sigma-Aldrich or Nacalai Tesque unless otherwise noted.

Animals

Mincle KO mice and enhanced GFP (*Egfp*) transgenic (Tg) mice on the C57BL/6J genetic background were kindly provided by Drs. Shizuo Akira and Masaru Okabe (Osaka University, Osaka, Japan), respectively (Okabe et al., 1997; Yamasaki et al., 2009). *Mincle* Tg mice on the C57BL/6J background ubiquitously overexpressing *Mincle* under the control of the cytomegalovirus early enhancer/chicken β actin (CAG) promoter were previously described (Miyake et al., 2015). 8-wk-old C57BL/6J WT mice were purchased from CLEA Japan. C57BL/6 mice congenic for the CD45 locus (B6-Ly5.1 mice) were bred and maintained at Sankyo Labo Service (Tsukuba, Japan). *Cx3cr1*^{CreERT2} mice (B6.129P2(C)-*Cx3cr1*$^{tm2.1(cre/ERT2)Jung}$/J) and *ROSA26*$^{tdTomato/tdTomato}$ mice (B6.Cg-*Gt(ROSA)26Sor*$^{tm9(CAG-tdTomato)Hze}$/J) were purchased from the Jackson Laboratory and were crossed to generate *Cx3cr1*$^{CreERT2/+}$:*ROSA26*$^{tdTomato/tdTomato}$ mice. They were maintained in a temperature-, humidity-, and light-controlled room (12-h light/dark cycles) and were allowed free access to water and standard chow (CE-2; 343.1 kcal per 100 g, 12.6% energy as fat; CLEA Japan). All animal experiments were approved by the Committee on the Ethics of Animal Experiments of Nagoya University (approval no. 19253).

Induction of renal ischemia–reperfusion injury

Renal ischemia–reperfusion injury was induced using 8–10-wk-old mice. Mice were anesthetized with pentobarbital (65 mg/kg body weight), and kidneys were exposed through small flank incisions. The left kidney pedicle was clamped for 30 min (with right nephrectomy) or 35 min (without right nephrectomy). After the clamp was released (reperfusion), the mice were observed for up to 14 d. During surgery, mice were placed on a 37°C heat pad. Serum BUN concentrations were determined with a biochemical analyzer, DRI-CHEM NX500V (Fujifilm).

Bone marrow transplantation experiments

Bone marrow transplantation experiments were performed as described (Tanaka et al., 2014). In brief, bone marrow cells obtained from donor mice were washed three times with cold PBS and injected intravenously (3.0×10^6 cells) into 7.5 Gy–irradiated 8-wk-old male recipient mice. After 4 wk, the substitution rate of bone marrow cells was determined by counting EGFP-positive cells in the peripheral blood, and then the mice were subjected to renal ischemia–reperfusion experiments. Reconstitution of macrophages was also examined using CD45.1 and CD45.2 mice for donors and recipients, respectively (Fig. S5). After 4 wk at steady state, the substitution rate of circulating monocytes (CD45$^+$ CD11b$^+$ CD115$^+$) and F4/80^{lo} macrophages (CD45$^+$ CD11b$^+$ F4/80^{lo}) was >95%, whereas that of F4/80^{hi} macrophages (CD45$^+$ CD11b$^+$ F4/80^{hi}) was ∼80%.

Lineage tracing experiments

Cx3cr1$^{CreERT2/+}$: *Rosa26*$^{tdTomato/tdTomato}$ mice were orally administered 100 mg/kg of tamoxifen for 5 consecutive days. Before and after administration, expression of tdTomato on circulating CX3CR1-expressing cells was determined using MACSQuant analyzer (Miltenyi Biotec). After 4 wk, these mice were subjected to renal ischemia–reperfusion injury and tdTomato expression in F4/80^{lo} and F4/80^{hi} macrophages from the injured kidney were evaluated using MACSQuant analyzer.

Histological analysis

For periodic acid–Schiff, naphthol AS-D chloroacetate esterase, and immunohistochemical stainings, kidneys were fixed with neutral-buffered formalin and embedded in paraffin. For immunofluorescent staining, paraformaldehyde-fixed kidneys were embedded in optimal cutting temperature compound and frozen in dry ice acetone. Immunostaining was performed as described (Tanaka et al., 2014) using the antibodies listed in Table S1. For detection of cholesterol, 0.05 mg/ml of Filipin III (Polysciences) was added to the sections. Apoptotic cells were detected by TUNEL assay using commercial kits (S7101, S7165; Merck). Quantitative analysis of TUNEL-positive cells was performed in 10 nonoverlapping visual fields (400× magnification) of each kidney cortex. Renal damage was evaluated in at least five nonoverlapping visual fields (200× magnification) of the kidney outer medulla. The ATN score was graded by cell necrosis, loss of brush border, cast formation, and tubule dilation (0: none; 1: <10%; 2: 11–25%; 3: 26–45%; 4: 46–75%; and 5: >76%) as previously reported (Yoshida et al., 2008). All samples were analyzed with a fluorescence microscope (BZ-X710; KEYENCE). The quantitative histological analysis was performed by two investigators who had no knowledge of the origin of the slides.

In situ hybridization

In situ hybridization for *Mincle* mRNA was performed as described (Tanaka et al., 2014). In brief, paraffin-embedded tissue blocks from kidneys were sectioned at 8 µm. The sections were hybridized with digoxigenin-labeled RNA probes specific for sense and antisense of *Mincle* (571–979 aa). The bound label was detected using NBT-BCIP, an alkaline phosphate color substrate. The sections were counterstained with Nuclear Fast red.

Quantitative real-time PCR

Quantitative real-time PCR was performed as described (Tanaka et al., 2014). In brief, total RNA was extracted from the tissues or cultured cells using Sepasol reagent, and 10 ng of cDNA was used for real-time PCR amplification with SYBR GREEN detection protocol in a thermal cycler (StepOne Plus; Thermo Fisher Scientific). Primers used in this study are listed in Table S2. Data were normalized to 36B4 levels and analyzed using the comparative cycle threshold method.

Western blotting analysis

Western blotting analysis was performed as described with slight modifications (Tanaka et al., 2014). Peritoneal macrophages were stimulated with Mincle ligands for 24 h and lysed in RIPA buffer (150 mM NaCl, 1% NP-40, 0.5% sodium deoxycholate, 0.1% SDS, and 50 mM Tris, pH 7.4) supplemented with Protease Inhibitor Cocktail (Merck) and Phosphatase Inhibitor Cocktail 2 and 3. Proteins were separated by SDS-PAGE and immunoblotted with anti-phospho Syk (Tyr525/526) antibody (diluted 1:500; #2710; Cell Signaling Technology) and anti-Syk antibody (diluted 1:1,000; #13198; Cell Signaling Technology) as primary antibody and anti-rabbit IgG, HRP-linked antibody (diluted 1:10,000; #7074; Cell Signaling Technology) as secondary antibody. Immunoblots were detected and analyzed with Immobilon Forte (Merck) and the ChemiDoc Imaging System (BioRad).

Flow cytometric analysis

For cell sorting, kidneys were digested in HBSS with calcium and magnesium supplemented with 1 mg/ml type 4 collagenase (Worthington) and 50 µg/ml DNaseI (Roche) using gentleMACS Dissociator (Miltenyi Biotec). After filtering through a 100-µm mesh, cells were washed and incubated with the antibodies listed in Table S3, sorted using FACSAriaIII (BD Biosciences), and used for mRNA expression analysis. For analysis of Mincle-expressing cells, kidneys were dispersed using the Minute Single Cell Isolation Kit (Invent Biotechnologies) and analyzed using MACSQuant analyzer and FlowJo V9 software (BD Biosciences) or sorted using FACSAriaIII. For analysis of phosphorylation of Syk, peritoneal macrophages were stimulated with Mincle ligands for 24 h and fixed with 4% paraformaldehyde and permeabilized by 90% methanol. Cells were incubated with the antibodies listed in Table S3 and analyzed using MACSQuant analyzer and FlowJo V9 software.

In vitro phagocytosis assay

Engulfment and binding assays were performed as described (Nakaya et al., 2017; Toda et al., 2012). Briefly, thymocytes were collected from female C57BL/6 mice and treated with 10 µM dexamethasone at 37°C for 5 h to induce apoptosis or heated at 55°C for 20 min to induce necrosis (Budai et al., 2019). Thymocytes were labeled with pHrodo Red succinimidyl ester or CellTracker Green CMFDA Dye (Thermo Fisher Scientific) for engulfment assay and binding assay, respectively. Peritoneal cells from *Mincle* KO and WT mice were stimulated with TDM for 24 h, and pHrodo-labeled thymocytes were added for 2 h at 37°C in DMEM containing 10% FBS for engulfment assay. CellTracker-labeled thymocytes were added for 2 h at room temperature in PBS containing 10% FBS for binding assay. APC-conjugated anti-mouse F4/80 antibody was added, and the cells were analyzed using MACSQuant analyzer. Engulfment and binding were determined as the percentage of pHrodo-positive cells and the percentage of CMFDA-positive cells in the F4/80-positive population, respectively. Debris phagocytosis assay was performed as described (Arai et al., 2016). Briefly, heat-killed mProx24, a mouse proximal tubular cell line (Takaya et al., 2003), was labeled with Fixable Viability Dye (FVD 660; Thermo Fischer Scientific) and sonicated for 30 s. Peritoneal macrophages were incubated with sonicated debris for 30 min, stained with FITC-conjugated anti-F4/80 antibody, and analyzed using MACSQuant analyzer.

Non-targeted metabolome analysis

The total lipids were extracted from the kidney with the Bligh and Dyer method (Bligh and Dyer, 1959). The lipids were applied

to the silica gel column (InertSep SI; GL Sciences) and eluted isocratically with chloroform and methanol. The fraction IR–9:1, which has high ligand activity, was used for further analysis. For nontargeted analysis, metabolome data obtained by orbitrap-type MS (Q-Exactive focus; Thermo Fisher Scientific) connected to an HPLC (UltiMate 3000 system; Thermo Fisher Scientific) with the discovery HS F5-3 column or an ion chromatography (ICS-5000+; Thermo Fisher Scientific) with the IonPac AS11-HC, 4-µm particle size column were analyzed. A Compound Discoverer 2.0 (Thermo Fisher Scientific) was used for the nontargeted metabolomics workflow as described (Miyajima et al., 2017).

Matrix-assisted laser desorption/ionization (MALDI)–MS imaging

MALDI imaging analyses were performed as described previously (Miyajima et al., 2017). Briefly, thin sections (8 µm) of the kidney prepared with a cryomicrotome (CM3050; Leica Microsystems) were attached to indium tin oxide–coated glass slides (Bruker Daltonics GmbH) and coated with 2,5-dihydroxy benzoic acid as the matrix (50 mg/ml, dissolved in 80% ethanol) by manually spraying with an artistic brush (Procon Boy FWA Platinum; Mr. Hobby). The matrix was simultaneously applied to multiple sections in order to maintain consistent analyte extraction and cocrystallization conditions. Data were acquired with an orbitrap MS coupled with an atmospheric pressure scanning microprobe MALDI ion source (AP-SMALDI10; TransMIT GmbH). Signals within a mass range between 700 and 900 were acquired with a mass resolving power of 70,000 at m/z 200. Thereafter, the spectral data were transformed to image data and analyzed using ImageQuest 1.0.1 (Thermo Fisher Scientific), SCiLS 2019a (Bruker Daltonics), and ImageJ 1.51 (National Institutes of Health) software.

LC-MS/MS

The amount of β-glucosylceramide in the kidney tissue extracts was quantified using LC-MS using orbitrap-type MS connected to an UltiMate 3000 RSLC system (Dionex; Thermo Scientific). The samples were resolved on the Accucore C18 column (2.1 × 150 mm, 2.6 µm; Thermo Fisher Scientific) using a step gradient with mobile phase A (10 mM $HCOONH_4$ in 50% acetonitrile [vol]; with 0.1% HCOOH [vol]) and mobile phase B (2 mM $HCOONH_4$ in acetonitrile/isopropanol/H_2O 10:88:2 [vol/vol/vol] with 0.02% HCOOH [vol]) at ratios of 65:35 (0 min), 40:60 (0–4 min), 15:85 (4–12 min), 0:100 (12–21 min), and 0:100 (21–41 min) at a flow rate of 0.4 ml/min. The Q-Exactive focus MS was operated under an electrospray ionization–positive mode for all detections. Full mass scan (m/z 70–1,000) was used at a resolution of 70,000 with data-dependent MS/MS measurement. The automatic gain control target was set at 3×10^6 ions, and the maximum ion injection time was 100 ms. Source ionization parameters were optimized with a spray voltage of 3 kV, and other parameters were as follows: transfer temperature at 370°C, S-Lens level at 45, heater temperature at 370°C, sheath gas at 60, and auxiliary gas at 20.

Screening for endogenous Mincle ligands

Endogenous Mincle ligands were screened using the 2B4–NFAT-GFP reporter cells expressing murine Mincle as described, with some modifications (Yamasaki et al., 2008). Cells were incubated in the lipid extract-coated 96-well plate, and after 18 h, propidium iodide was added to gate out dead cells, and the cell samples were analyzed using a MACSQuant analyzer. To evaluate the synergistic effect of β-glucosylceramide and cholesterol on *Il6* mRNA expression, RAW267 macrophages or peritoneal macrophages from *Mincle* KO and WT mice were incubated in the lipid-coated 24-well plate, and after 24 h, the cells were harvested for mRNA analysis.

cDNA microarray analysis

cDNA microarray analysis was performed using Affymetrix GeneChip Mouse Genome 430 2.0 Arrays as described previously (Tanaka et al., 2014). In this study, genes with an average fold change ≥3.0 together with a label of "present" and "increased" were considered to be differentially up-regulated. Genes with an average fold change ≤0.7 together with a label of present and "decreased" were considered to be differentially down-regulated. Pathway and gene ontology analyses were performed using DAVID GO_BP. The raw data are available on the web site of the Gene Expression Omnibus at the National Center for Biotechnology Information (GEO accession no. GSE153321).

Statistical analysis

Data are means ± SEM, and $P < 0.05$ was considered statistically significant. Statistical analysis was performed using ANOVA, followed by the Tukey-Kramer test. Unpaired *t* test was used to compare two groups. All experiments were repeated more than three times unless otherwise noted.

Online supplemental material

Fig. S1 shows the evaluation of renal inflammation and injury on day 1 after renal ischemia–reperfusion. Fig. S2 shows microarray analysis of the kidney after renal ischemia–reperfusion. Fig. S3 shows screening for the endogenous Mincle ligand in injured kidney after renal ischemia–reperfusion. Fig. S4 shows the potential role of Mincle in cell death–triggered sustained inflammation following AKI. Fig. S5 shows the effect of bone marrow transplantation on reconstitution of circulating monocytes and renal macrophages. Table S1 lists all the antibodies, dyes, incubation time, and concentrations used in histological analyses. Table S2 lists the primers used to detect mRNAs. Table S3 lists all the antibodies used in flow cytometric analyses.

Acknowledgments

The authors thank Dr. Makoto Arita (Keio University) for technical advice for lipidomics analysis, Dr. Michio Nakaya for phagocytosis analysis, and Drs. Shizuo Akira and Masaru Okabe for their generous gifts of *Mincle* KO mice and *Egfp* Tg mice. We also thank the members of the Suganami laboratory for helpful discussion and the Center for Animal Research and Education (CARE), Nagoya University, for support with animal experiments.

This work was supported in part by Grants-in-Aid for Scientific Research from the Ministry of Education, Culture, Sports, Science and Technology of Japan (17H05500, 20H03447, 20H05503, and 20H04944 to T. Suganami and 18K08508 to M. Tanaka) and the Japan Agency for Medical Research and

Development (Core Research for Evolutional Science and Technology; JP19gm1210009s0101 to T. Suganami and JP19gm0610011h9905 to Y. Ogawa). The imaging metabolomics platform was established by the Japan Science and Technology Agency Exploratory Research for Advanced Technology Suematsu Gas Biology Project led by M. Suematsu until March 2015. This study was also supported by research grants from The Hori Sciences and Arts Foundation, the Takeda Science Foundation, The NOVARTIS Foundation (Japan) for the Promotion of Science (to T. Suganami), the Terumo Life Science Foundation, The Ichiro Kanehara Foundation for the Promotion of Medical Sciences and Medical Care, the ONO Medical Research Foundation, the Ishibashi Yukiko Foundation, and the Daiichi Sankyo Foundation of Life Science (to M. Tanaka) and the Aichi Kidney Foundation (to M. Saka-Tanaka).

Author contributions: M. Tanaka, M. Saka-Tanaka, and T. Suganami designed the research and wrote the manuscript. M. Tanaka and M. Saka-Tanaka did animal experiments with ischemia–reperfusion injury, analyzed data, and generated the figures. M. Tanaka, M. Saka-Tanaka, and K. Ochi performed and analyzed flow cytometry. M. Saka-Tanaka and K. Fujieda performed in vitro experiments including the phagocytosis assays. M. Saka-Tanaka, K. Fujieda, and H. Kohda performed histological analysis. T. Miyamoto, Y. Sugiura, M. Suematsu, S. Aoe, A. Matsumoto, and T. Miyazawa performed lipidomics analysis and imaging MS. M. Saka-Tanaka and Y. Miyamoto performed transcriptome analysis. M. Tanaka, K. Ochi, T. Miyamoto, and S. Yamasaki performed screening for endogenous Mincle ligands. A. Ito, S. Yamasaki, N. Tsuboi, S. Maruyama, and Y. Ogawa helped with experimental design and edited the manuscript. T. Suganami and Y. Ogawa supervised the whole study.

Disclosures: N. Tsuboi reported grants from Chugai Pharmaceutical Co., Ltd., personal fees from Chugai Pharmaceutical Co., Ltd., personal fees from Kyowa Kirin Co., Ltd., personal fees from Mochida Pharmaceutical Co., Ltd., personal fees from Sanofi K.K., personal fees from Eisai Co., Ltd., grants from The Ministry of Education, Culture, Sports, Science and Technology, Japan, grants from Grant-in-Aid from Japan Research Committee of the Ministry of Health, Labour, and Welfare for Intractable Renal Disease, grants from Japan Agency for Medical Research and Development, grants from Asahi Kasei Medical Co., Ltd., and grants from Novartis Pharma K.K. outside the submitted work. No other disclosures were reported.

Submitted: 26 November 2019
Revised: 8 June 2020
Accepted: 7 July 2020

References

Arai, S., K. Kitada, T. Yamazaki, R. Takai, X. Zhang, Y. Tsugawa, R. Sugisawa, A. Matsumoto, M. Mori, Y. Yoshihara, et al. 2016. Apoptosis inhibitor of macrophage protein enhances intraluminal debris clearance and ameliorates acute kidney injury in mice. *Nat. Med.* 22:183–193. https://doi.org/10.1038/nm.4012

Baek, J.H.. 2019. The impact of versatile macrophage functions on acute kidney injury and its outcomes. *Front. Physiol.* 10:1016. https://doi.org/10.3389/fphys.2019.01016

Basile, D.P., M.D. Anderson, and T.A. Sutton. 2012. Pathophysiology of acute kidney injury. *Compr. Physiol.* 2:1303–1353. https://doi.org/10.1002/cphy.c110041

Behler-Janbeck, F., T. Takano, R. Maus, J. Stolper, D. Jonigk, M. Tort Tarrés, T. Fuehner, A. Prasse, T. Welte, M.S. Timmer, et al. 2016. C-type lectin Mincle recognizes glucosyl-diacylglycerol of *Streptococcus pneumoniae* and plays a protective role in pneumococcal pneumonia. *PLoS Pathog.* 12. e1006038. https://doi.org/10.1371/journal.ppat.1006038

Bligh, E.G., and W.J. Dyer. 1959. A rapid method of total lipid extraction and purification. *Can. J. Biochem. Physiol.* 37:911–917. https://doi.org/10.1139/o59-099

Budai, Z., L. Ujlaky-Nagy, G.N. Kis, M. Antal, C. Bankó, Z. Bacsó, Z. Szondy, and Z. Sarang. 2019. Macrophages engulf apoptotic and primary necrotic thymocytes through similar phosphatidylserine-dependent mechanisms. *FEBS Open Bio.* 9:446–456. https://doi.org/10.1002/2211-5463.12584

Chen, G.Y., and G. Nuñez. 2010. Sterile inflammation: sensing and reacting to damage. *Nat. Rev. Immunol.* 10:826–837. https://doi.org/10.1038/nri2873

Clements, M., M. Gershenovich, C. Chaber, J. Campos-Rivera, P. Du, M. Zhang, S. Ledbetter, and A. Zuk. 2016. Differential Ly6C expression after renal ischemia-reperfusion identifies unique macrophage populations. *J. Am. Soc. Nephrol.* 27:159–170. https://doi.org/10.1681/ASN.2014111138

Ferenbach, D.A., and J.V. Bonventre. 2015. Mechanisms of maladaptive repair after AKI leading to accelerated kidney ageing and CKD. *Nat. Rev. Nephrol.* 11:264–276. https://doi.org/10.1038/nrneph.2015.3

Greco, S.H., A. Torres-Hernandez, A. Kalabin, C. Whiteman, R. Rokosh, S. Ravirala, A. Ochi, J. Gutierrez, M.A. Salyana, V.R. Mani, et al. 2016. Mincle signaling promotes Con A hepatitis. *J. Immunol.* 197:2816–2827. https://doi.org/10.4049/jimmunol.1600598

Haider, M., I.M. Dambuza, P. Asamaphan, M. Stappers, D. Reid, S. Yamasaki, G.D. Brown, N.A.R. Gow, and L.P. Erwig. 2019. The pattern recognition receptors dectin-2, mincle, and FcRγ impact the dynamics of phagocytosis of *Candida, Saccharomyces, Malassezia*, and *Mucor* species. *PLoS One.* 14. e0220867. https://doi.org/10.1371/journal.pone.0220867

Huen, S.C., and L.G. Cantley. 2015. Macrophage-mediated injury and repair after ischemic kidney injury. *Pediatr. Nephrol.* 30:199–209. https://doi.org/10.1007/s00467-013-2726-y

Ishikawa, E., T. Ishikawa, Y.S. Morita, K. Toyonaga, H. Yamada, O. Takeuchi, T. Kinoshita, S. Akira, Y. Yoshikai, and S. Yamasaki. 2009. Direct recognition of the mycobacterial glycolipid, trehalose dimycolate, by C-type lectin Mincle. *J. Exp. Med.* 206:2879–2888. https://doi.org/10.1084/jem.20091750

Ito, A., C. Hong, X. Rong, X. Zhu, E.J. Tarling, P.N. Hedde, E. Gratton, J. Parks, and P. Tontonoz. 2015. LXRs link metabolism to inflammation through Abca1-dependent regulation of membrane composition and TLR signaling. *eLife.* 4. e08009. https://doi.org/10.7554/eLife.08009

Itoh, M., H. Kato, T. Suganami, K. Konuma, Y. Marumoto, S. Terai, H. Sakugawa, S. Kanai, M. Hamaguchi, T. Fukaishi, et al. 2013. Hepatic crown-like structure: a unique histological feature in non-alcoholic steatohepatitis in mice and humans. *PLoS One.* 8. e82163. https://doi.org/10.1371/journal.pone.0082163

Itoh, M., T. Suganami, H. Kato, S. Kanai, I. Shirakawa, T. Sakai, T. Goto, M. Asakawa, I. Hidaka, H. Sakugawa, et al. 2017. CD11c^{+} resident macrophages drive hepatocyte death-triggered liver fibrosis in a murine model of nonalcoholic steatohepatitis. *JCI Insight.* 2. e92902. https://doi.org/10.1172/jci.insight.92902

Kasikara, C., A.C. Doran, B. Cai, and I. Tabas. 2018. The role of non-resolving inflammation in atherosclerosis. *J. Clin. Invest.* 128:2713–2723. https://doi.org/10.1172/JCI97950

Kiyotake, R., M. Oh-Hora, E. Ishikawa, T. Miyamoto, T. Ishibashi, and S. Yamasaki. 2015. Human Mincle binds to cholesterol crystals and triggers innate immune responses. *J. Biol. Chem.* 290:25322–25332. https://doi.org/10.1074/jbc.M115.645234

Kojima, Y., J.P. Volkmer, K. McKenna, M. Civelek, A.J. Lusis, C.L. Miller, D. Direnzo, V. Nanda, J. Ye, A.J. Connolly, et al. 2016. CD47-blocking antibodies restore phagocytosis and prevent atherosclerosis. *Nature.* 536:86–90. https://doi.org/10.1038/nature18935

Kostarnoy, A.V., P.G. Gancheva, B. Lepenies, A.I. Tukhvatulin, A.S. Dzharullaeva, N.B. Polyakov, D.A. Grumov, D.A. Egorova, A.Y. Kulibin, M.A. Bobrov, et al. 2017. Receptor Mincle promotes skin allergies and is capable of recognizing cholesterol sulfate. *Proc. Natl. Acad. Sci. USA.* 114:E2758–E2765. https://doi.org/10.1073/pnas.1611665114

Lee, S., S. Huen, H. Nishio, S. Nishio, H.K. Lee, B.S. Choi, C. Ruhrberg, and L.G. Cantley. 2011. Distinct macrophage phenotypes contribute to kidney injury and repair. *J. Am. Soc. Nephrol.* 22:317–326. https://doi.org/10.1681/ASN.2009060615

Lee, W.B., J.S. Kang, J.J. Yan, M.S. Lee, B.Y. Jeon, S.N. Cho, and Y.J. Kim. 2012. Neutrophils promote mycobacterial trehalose dimycolate-induced lung

inflammation via the Mincle pathway. *PLoS Pathog*. 8. e1002614. https://doi.org/10.1371/journal.ppat.1002614

Linkermann, A., G. Chen, G. Dong, U. Kunzendorf, S. Krautwald, and Z. Dong. 2014. Regulated cell death in AKI. *J. Am. Soc. Nephrol*. 25:2689–2701. https://doi.org/10.1681/ASN.2014030262

Lu, Q., and G. Lemke. 2001. Homeostatic regulation of the immune system by receptor tyrosine kinases of the Tyro 3 family. *Science*. 293:306–311. https://doi.org/10.1126/science.1061663

Lumeng, C.N., J.B. DelProposto, D.J. Westcott, and A.R. Saltiel. 2008. Phenotypic switching of adipose tissue macrophages with obesity is generated by spatiotemporal differences in macrophage subtypes. *Diabetes*. 57:3239–3246. https://doi.org/10.2337/db08-0872

Lv, L.L., P.M.K. Tang, C.J. Li, Y.K. You, J. Li, X.R. Huang, J. Ni, M. Feng, B.C. Liu, and H.Y. Lan. 2017. The pattern recognition receptor, Mincle, is essential for maintaining the M1 macrophage phenotype in acute renal inflammation. *Kidney Int*. 91:587–602. https://doi.org/10.1016/j.kint.2016.10.020

Matsumoto, M., T. Tanaka, T. Kaisho, H. Sanjo, N.G. Copeland, D.J. Gilbert, N.A. Jenkins, and S. Akira. 1999. A novel LPS-inducible C-type lectin is a transcriptional target of NF-IL6 in macrophages. *J. Immunol*. 163: 5039–5048.

Meng, X.M., P.M. Tang, J. Li, and H.Y. Lan. 2015. Macrophage phenotype in kidney injury and repair. *Kidney Dis*. 1:138–146. https://doi.org/10.1159/000431214

Miyajima, M., B. Zhang, Y. Sugiura, K. Sonomura, M.M. Guerrini, Y. Tsutsui, M. Maruya, A. Vogelzang, K. Chamoto, K. Honda, et al. 2017. Metabolic shift induced by systemic activation of T cells in PD-1-deficient mice perturbs brain monoamines and emotional behavior. *Nat. Immunol*. 18: 1342–1352. https://doi.org/10.1038/ni.3867

Miyake, K.. 2007. Innate immune sensing of pathogens and danger signals by cell surface Toll-like receptors. *Semin. Immunol*. 19:3–10. https://doi.org/10.1016/j.smim.2006.12.002

Miyake, Y., O.H. Masatsugu, and S. Yamasaki. 2015. C-Type lectin receptor MCL facilitates Mincle expression and signaling through complex formation. *J. Immunol*. 194:5366–5374. https://doi.org/10.4049/jimmunol.1402429

Mulay, S.R., A. Linkermann, and H.J. Anders. 2016. Necroinflammation in kidney disease. *J. Am. Soc. Nephrol*. 27:27–39. https://doi.org/10.1681/ASN.2015040405

Murano, I., G. Barbatelli, V. Parisani, C. Latini, G. Muzzonigro, M. Castellucci, and S. Cinti. 2008. Dead adipocytes, detected as crown-like structures, are prevalent in visceral fat depots of genetically obese mice. *J. Lipid Res*. 49:1562–1568. https://doi.org/10.1194/jlr.M800019-JLR200

Nagata, S., and M. Tanaka. 2017. Programmed cell death and the immune system. *Nat. Rev. Immunol*. 17:333–340. https://doi.org/10.1038/nri.2016.153

Nagata, M., Y. Izumi, E. Ishikawa, R. Kiyotake, R. Doi, S. Iwai, Z. Omahdi, T. Yamaji, T. Miyamoto, T. Bamba, et al. 2017. Intracellular metabolite β-glucosylceramide is an endogenous Mincle ligand possessing immunostimulatory activity. *Proc. Natl. Acad. Sci. USA*. 114:E3285–E3294. https://doi.org/10.1073/pnas.1618133114

Nakaya, M., K. Watari, M. Tajima, T. Nakaya, S. Matsuda, H. Ohara, H. Nishihara, H. Yamaguchi, A. Hashimoto, M. Nishida, et al. 2017. Cardiac myofibroblast engulfment of dead cells facilitates recovery after myocardial infarction. *J. Clin. Invest*. 127:383–401. https://doi.org/10.1172/JCI83822

Okabe, M., M. Ikawa, K. Kominami, T. Nakanishi, and Y. Nishimune. 1997. 'Green mice' as a source of ubiquitous green cells. *FEBS Lett*. 407: 313–319. https://doi.org/10.1016/S0014-5793(97)00313-X

Pahari, S., S. Negi, M. Aqdas, E. Arnett, L.S. Schlesinger, and J.N. Agrewala. 2020. Induction of autophagy through CLEC4E in combination with TLR4: an innovative strategy to restrict the survival of *Mycobacterium tuberculosis*. *Autophagy*. 16:1021–1043. https://doi.org/10.1080/15548627.2019.1658436

Patin, E.C., A.C. Geffken, S. Willcocks, C. Leschczyk, A. Haas, F. Nimmerjahn, R. Lang, T.H. Ward, and U.E. Schaible. 2017a. Trehalose dimycolate interferes with FcγR-mediated phagosome maturation through Mincle, SHP-1 and FcγRIIB signalling. *PLoS One*. 12:e0174973. https://doi.org/10.1371/journal.pone.0174973

Patin, E.C., S.J. Orr, and U.E. Schaible. 2017b. Macrophage inducible C-type lectin as a multifunctional player in immunity. *Front. Immunol*. 8:861. https://doi.org/10.3389/fimmu.2017.00861

Reed-Geaghan, E.G., A.L. Croxford, B. Becher, and G.E. Landreth. 2020. Plaque-associated myeloid cells derive from resident microglia in an Alzheimer's disease model. *J. Exp. Med*. 217. e20191374. https://doi.org/10.1084/jem.20191374

Sato, Y., and M. Yanagita. 2018. Immune cells and inflammation in AKI to CKD progression. *Am. J. Physiol. Renal Physiol*. 315:F1501–F1512. https://doi.org/10.1152/ajprenal.00195.2018

Seifert, L., G. Werba, S. Tiwari, N.N. Giao Ly, S. Alothman, D. Alqunaibit, A. Avanzi, R. Barilla, D. Daley, S.H. Greco, et al. 2016. The necrosome promotes pancreatic oncogenesis via CXCL1 and Mincle-induced immune suppression. *Nature*. 532:245–249. https://doi.org/10.1038/nature17403

Serhan, C.N., S.D. Brain, C.D. Buckley, D.W. Gilroy, C. Haslett, L.A.J. O'Neill, M. Perretti, A.G. Rossi, and J.L. Wallace. 2007. Resolution of inflammation: state of the art, definitions and terms. *FASEB J*. 21:325–332. https://doi.org/10.1096/fj.06-7227rev

Sharma, A., T.J. Simonson, C.N. Jondle, B.B. Mishra, and J. Sharma. 2017. Mincle-mediated neutrophil extracellular trap formation by regulation of autophagy. *J. Infect. Dis*. 215:1040–1048. https://doi.org/10.1093/infdis/jix072

Takaya, K., D. Koya, M. Isono, T. Sugimoto, T. Sugaya, A. Kashiwagi, and M. Haneda. 2003. Involvement of ERK pathway in albumin-induced MCP-1 expression in mouse proximal tubular cells. *Am. J. Physiol. Renal Physiol*. 284:F1037–F1045. https://doi.org/10.1152/ajprenal.00230.2002

Tanaka, M., K. Ikeda, T. Suganami, C. Komiya, K. Ochi, I. Shirakawa, M. Hamaguchi, S. Nishimura, I. Manabe, T. Matsuda, et al. 2014. Macrophage-inducible C-type lectin underlies obesity-induced adipose tissue fibrosis. *Nat. Commun*. 5:4982. https://doi.org/10.1038/ncomms5982

Toda, S., R. Hanayama, and S. Nagata. 2012. Two-step engulfment of apoptotic cells. *Mol. Cell. Biol*. 32:118–125. https://doi.org/10.1128/MCB.05993-11

Wei, Q., G. Dong, J.K. Chen, G. Ramesh, and Z. Dong. 2013. Bax and Bak have critical roles in ischemic acute kidney injury in global and proximal tubule-specific knockout mouse models. *Kidney Int*. 84:138–148. https://doi.org/10.1038/ki.2013.68

Wells, C.A., J.A. Salvage-Jones, X. Li, K. Hitchens, S. Butcher, R.Z. Murray, A.G. Beckhouse, Y.L. Lo, S. Manzanero, C. Cobbold, et al. 2008. The macrophage-inducible C-type lectin, mincle, is an essential component of the innate immune response to *Candida albicans*. *J. Immunol*. 180: 7404–7413. https://doi.org/10.4049/jimmunol.180.11.7404

Yamasaki, S., E. Ishikawa, M. Sakuma, H. Hara, K. Ogata, and T. Saito. 2008. Mincle is an ITAM-coupled activating receptor that senses damaged cells. *Nat. Immunol*. 9:1179–1188. https://doi.org/10.1038/ni.1651

Yamasaki, S., M. Matsumoto, O. Takeuchi, T. Matsuzawa, E. Ishikawa, M. Sakuma, H. Tateno, J. Uno, J. Hirabayashi, Y. Mikami, et al. 2009. C-type lectin Mincle is an activating receptor for pathogenic fungus, Malassezia. *Proc. Natl. Acad. Sci. USA*. 106:1897–1902. https://doi.org/10.1073/pnas.0805177106

Yoshida, T., H. Sugiura, M. Mitobe, K. Tsuchiya, S. Shirota, S. Nishimura, S. Shiohira, H. Ito, K. Nobori, S.R. Gullans, et al. 2008. ATF3 protects against renal ischemia-reperfusion injury. *J. Am. Soc. Nephrol*. 19: 217–224. https://doi.org/10.1681/ASN.2005111155

Zhou, H., M. Yu, J. Zhao, B.N. Martin, S. Roychowdhury, M.R. McMullen, E. Wang, P.L. Fox, S. Yamasaki, L.E. Nagy, et al. 2016. IRAKM-Mincle axis links cell death to inflammation: Pathophysiological implications for chronic alcoholic liver disease. *Hepatology*. 64:1978–1993. https://doi.org/10.1002/hep.28811

JEM

Supplemental material

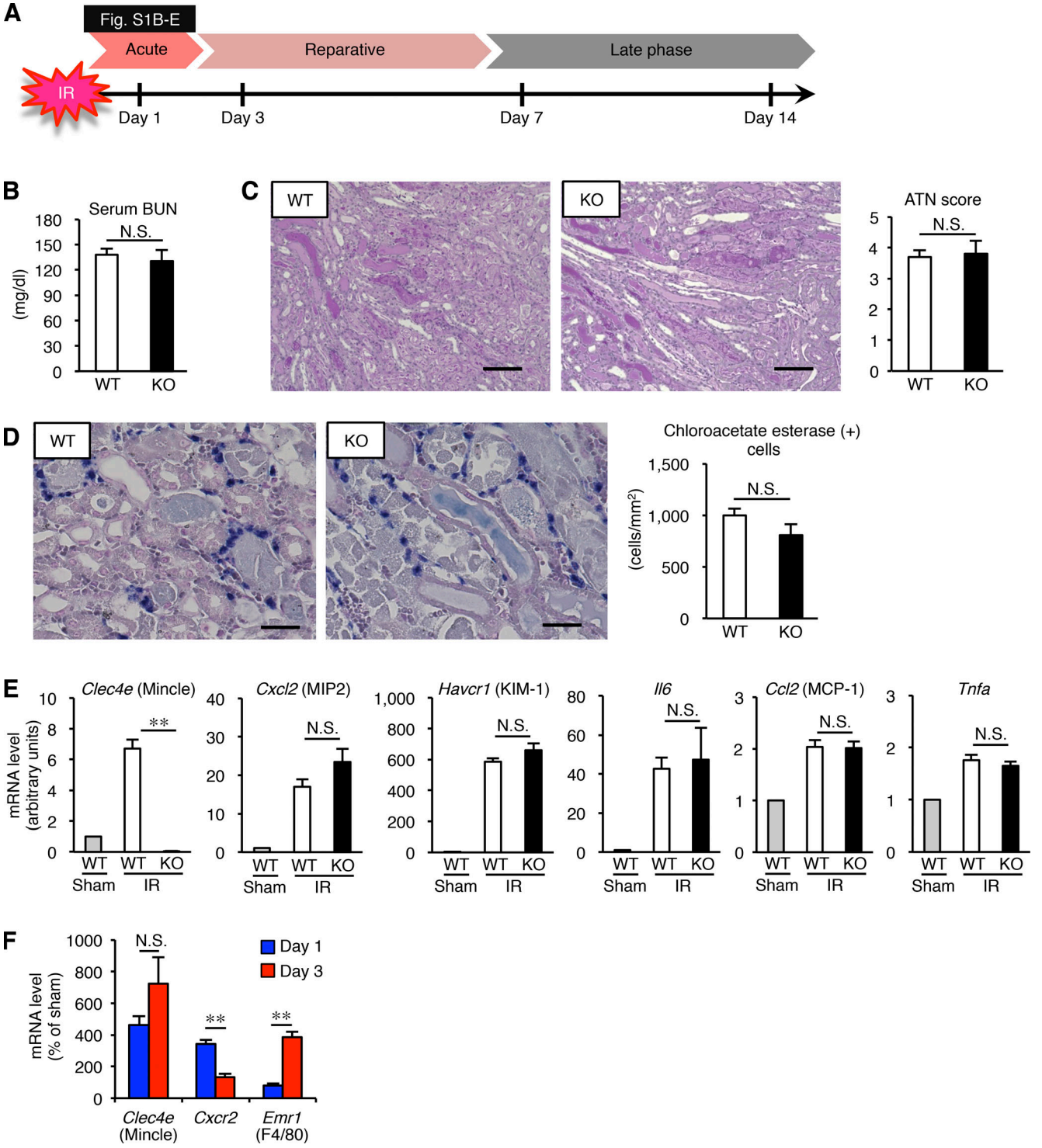

Figure S1. **Evaluation of renal inflammation and injury on day 1 after renal ischemia–reperfusion. (A)** Experimental time course of this study. **(B–E)** *Mincle*-deficient (KO) and WT mice were subjected to renal ischemia–reperfusion injury (ischemia for 30 min) after resection of the right kidney and were analyzed on day 1. **(B)** Serum BUN concentrations. Values are mean ± SEM. **(C)** Representative images of periodic acid–Schiff staining of the kidney outer medulla and ATN scores. Scale bars, 100 µm. Values are mean ± SEM. **(D)** Representative images of naphthol AS-D chloroacetate esterase staining (for neutrophils) of the kidney outer medulla and the number of chloroacetate esterase–positive cells. Scale bars, 100 µm. Values are mean ± SEM. **(E)** mRNA expression of the genes related to macrophages, inflammation, and tubular injury. WT mice, $n = 9$; KO mice. Values are mean ± SEM. $n = 7$. **, $P < 0.01$; ANOVA. **(F)** mRNA expression of *Clec4e* (Mincle), *Cxcr2* (a marker for neutrophils), and *Emr1* (F4/80, a marker for macrophages) after renal ischemia–reperfusion injury in WT mice. Values are mean ± SEM. $n = 6$. **, $P < 0.01$; unpaired *t* test. Data shown are representative of at least three independent experiments. N.S., not significant.

Figure S2. **Microarray analysis of the kidney after renal ischemia–reperfusion. (A)** Venn diagrams illustrating the up-regulated genes predominantly in the injured kidney of WT mice. Microarray analysis was performed on days 1 and 3 after renal ischemia–reperfusion. The overlap between the genes up-regulated in injured kidney versus sham kidney in WT mice and the genes down-regulated in injured kidney in KO mice versus WT mice are shown. **(B)** Gene ontology (GO) enrichment analysis. 58 genes, predominantly up-regulated in the injured kidney of WT mice compared with KO mice on day 3, were analyzed using DAVID Bioinformatics Resources, and the top 20 GO terms are shown.

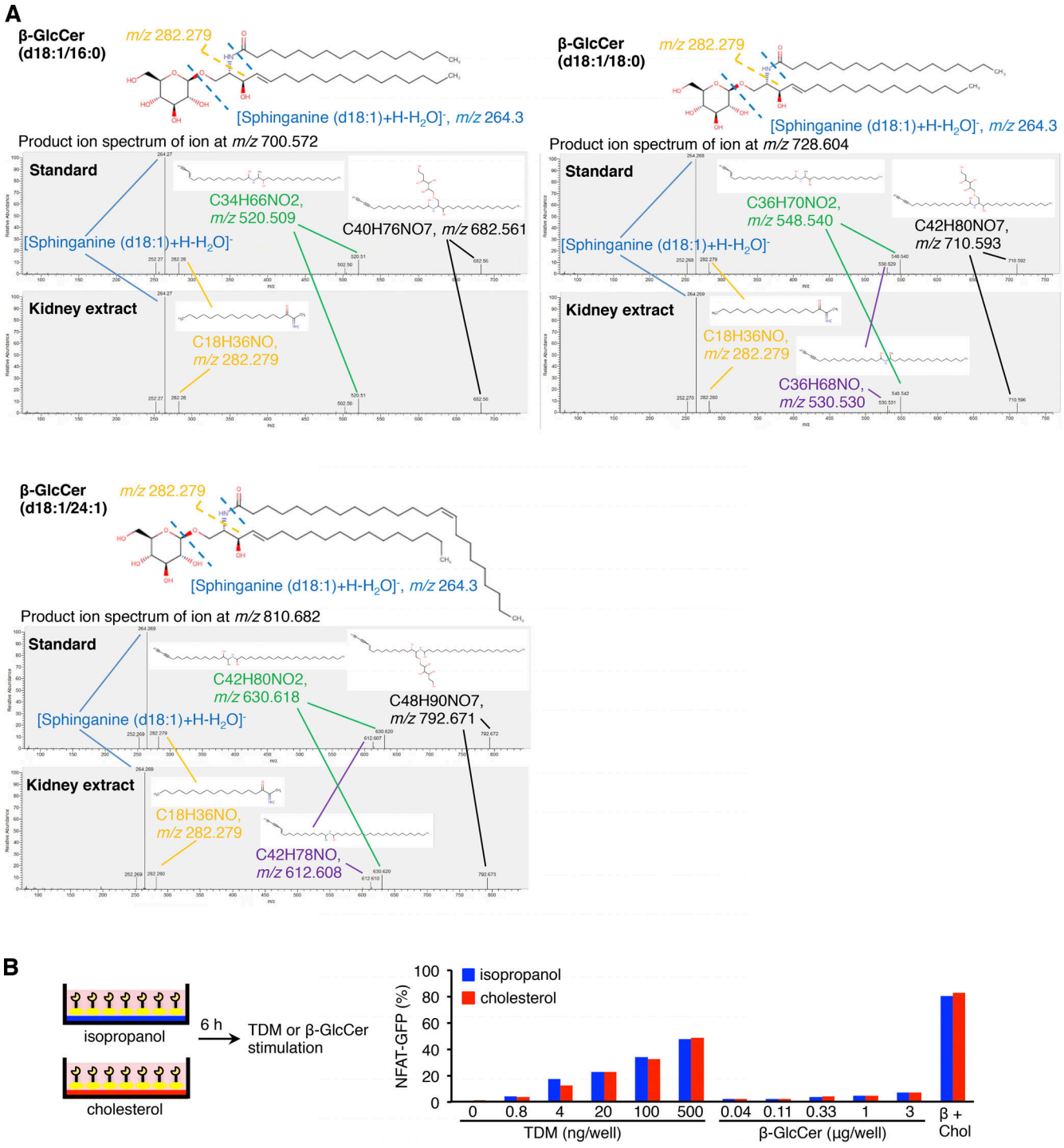

Figure S3. **Screening for endogenous Mincle ligand in injured kidney after renal ischemia–reperfusion. (A)** MS/MS spectra of each β-glucosylceramide standard and kidney extract on day 3 after ischemia–reperfusion injury; C16:0 (m/z 700.572), C18:0 (m/z 728.604), and C24:1 (m/z 810.682) in the positive-ion mode. **(B)** Effect of sequential stimulation with free cholesterol and β-GlcCer on reporter cell activity. After incubation with free cholesterol (5 μg/well, 96-well plate) for 6 h, the reporter cells were stimulated with β-GlcCer (d18:1/24:1; 0.04–3 μg/well) for an additional 18 h. As positive controls, reporter cells were stimulated with TDM (0–0.5 μg/well) or β-GlcCer (d18:1/24:1; 1 μg/well, 96-well plate) in the presence of free cholesterol (5 μg/well, 96-well plate) for 24 h. Chol, cholesterol.

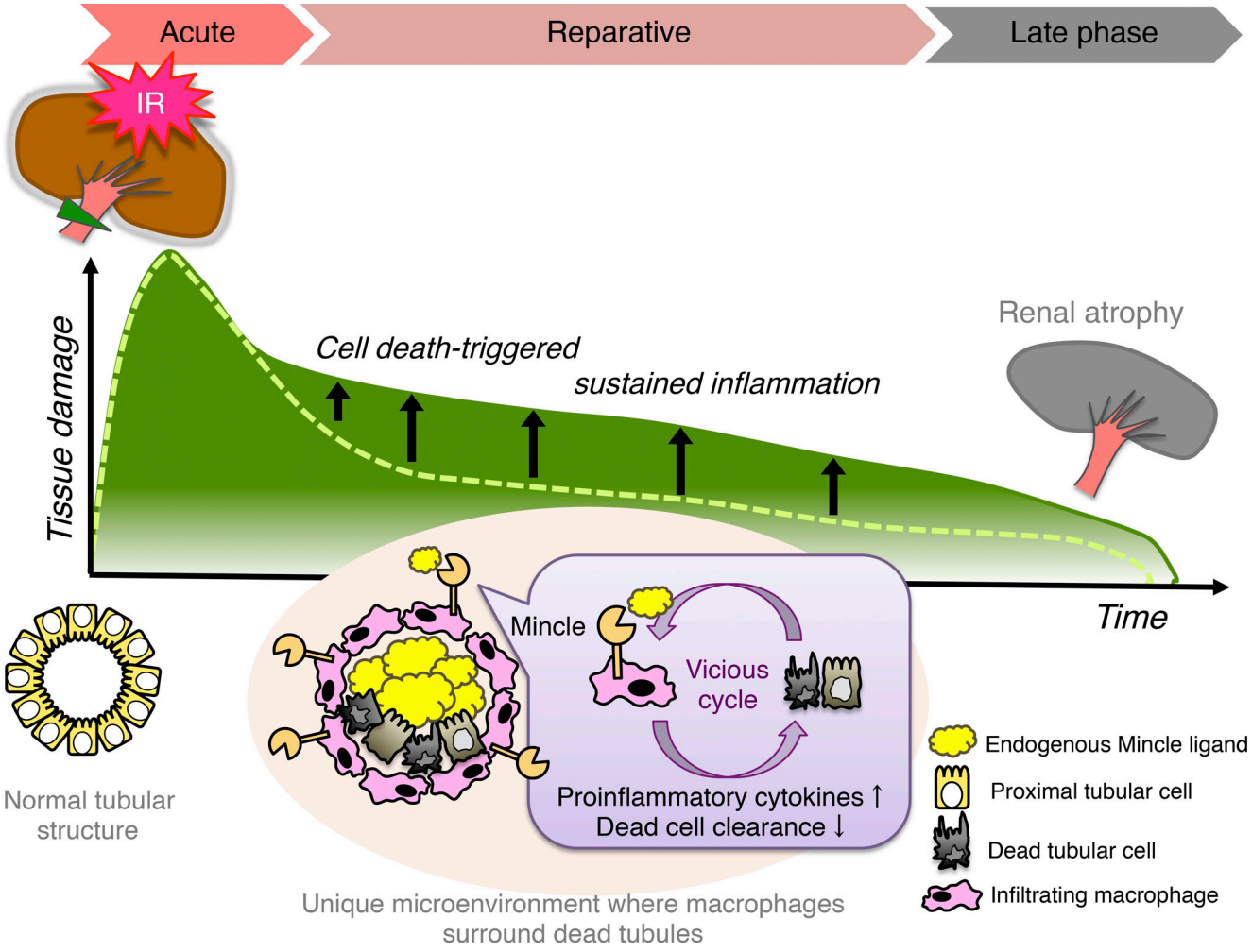

Figure S4. **Potential role of Mincle in cell death–triggered sustained inflammation following AKI.** A small cluster of Mincle-expressing macrophages aggregate around dead tubules in the injured area after renal ischemia–reperfusion, where Mincle induces proinflammatory cytokine production and inhibits dead cell clearance, thereby aggravating a vicious cycle of chronic inflammation. Thus, compared to KO mice (dashed line), WT mice show cell death–triggered sustained inflammation, leading to renal atrophy (green line). Our data also suggest that β-glucosylceramide derived from dead tubules in combination with free cholesterol is an endogenous ligand for Mincle. This study reveals a novel molecular mechanism underlying cell death–triggered sustained inflammation that promotes the AKI-to-CKD transition.

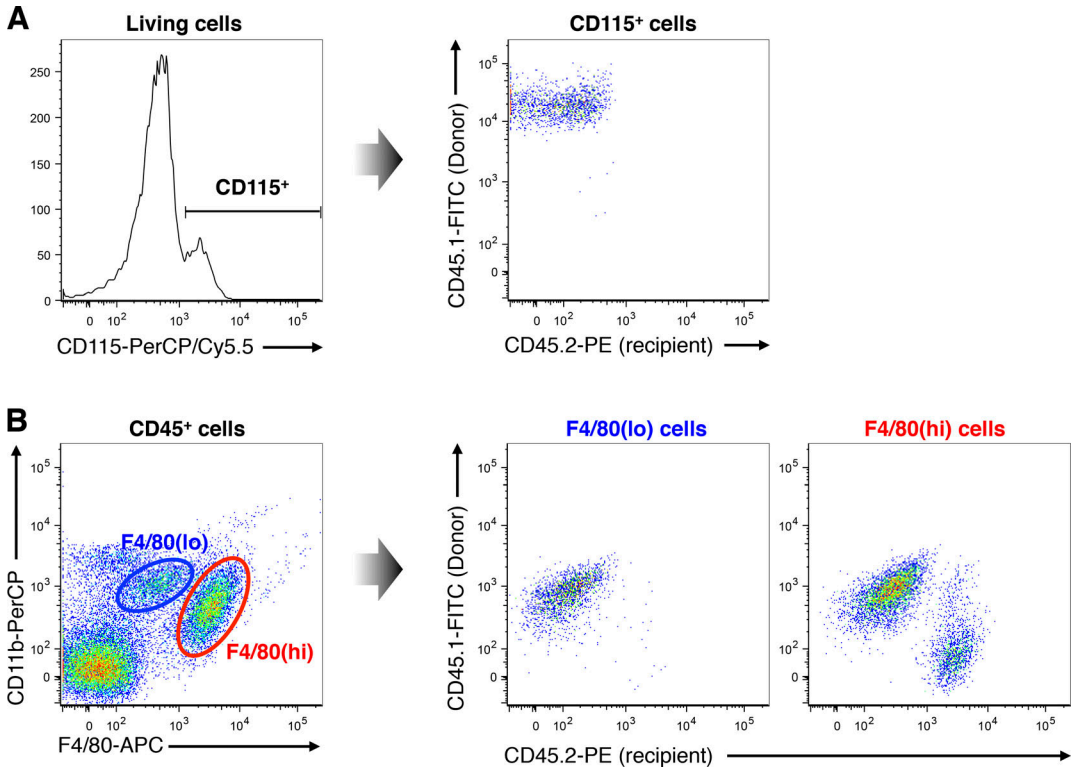

Figure S5. **Effect of bone marrow transplantation on reconstitution of circulating monocytes and renal macrophages. (A and B)** Reconstitution of monocytes/macrophages was examined using CD45.1 and CD45.2 mice for donors and recipients, respectively. CD45.2 recipient mice were irradiated with 7.5 Gy of x ray and received bone marrow cells from CD45.1 donor mice. After 4 wk of bone marrow transplantation, reconstitution was determined using CD45.1 and CD45.2 antibodies. Representative plots of circulating CD115-positive monocytes (A) and renal macrophages (B).

Tables S1–S3 are provided online as separate Word documents. Table S1 lists antibodies, dyes, incubation time, and concentration used in the histological analyses. Table S2 lists the primers used to detect mRNAs. Table S3 lists all the antibodies used in the flow cytometric analyses.